Title: Drosophila Ca_V2 channels harboring human migraine mutations cause synapse hyperexcitability that can be suppressed by inhibition of a Ca^{2+} store release pathway

Short Title: Drosophila models of Ca_V2 migraine mutations

Authors and Affiliations:

Douglas J. Brusich [1,4,5], Ashlyn M. Spring [1,2,6], Thomas D. James [1,3], Timothy H. Helms [1,7], C. Andrew Frank [1,2,3]

[1] – Department of Anatomy and Cell Biology, University of Iowa Carver College of Medicine, Iowa City, IA 52242

[2] – Interdisciplinary Graduate Program in Genetics, University of Iowa, Iowa City, IA 52242

[3] – Interdisciplinary Graduate Program in Neuroscience, University of Iowa, Iowa City, IA 52242

[4] – Present Address: Biology Department, Wartburg College, Waverly, IA 50677

[5] – Address as of August 2017: Human Biology, University of Wisconsin-Green Bay, Green Bay, WI 54311

[6] – Present Address: Department of Biology, University of North Carolina, Chapel Hill, NC 27599

[7] – Present Address: Department of Veterinary Biosciences, Ohio State University, Columbus, OH 43210

Address for Correspondence: C. Andrew Frank. Department of Anatomy and Cell Biology, University of Iowa Carver College of Medicine, 51 Newton Road, 1-661A. Iowa City, IA 52242. USA. andy-frank@uiowa.edu

ABSTRACT

Gain-of-function mutations in the human $Ca_V2.1$ gene *CACNA1A* cause familial hemiplegic migraine type 1 (FHM1). To characterize cellular problems potentially triggered by $Ca_V2.1$ gains of function, we engineered mutations encoding well-known FHM1 amino-acid substitutions S218L (SL) and R192Q (RQ) into transgenes of *Drosophila melanogaster* Ca_V2/*cacophony*. We expressed the transgenes pan-neuronally. Phenotypes were mild for RQ-expressing animals. By contrast, single mutant SL- and double mutant (DM) SL, RQ-expressing animals showed severe phenotypes, including sharply decreased viability. By electrophysiology, SL- and DM-expressing neuromuscular junctions (NMJs) exhibited enhanced evoked discharges, epileptiform supernumerary discharges when single electrical pulses were applied to the motor nerves, and a dramatic increase in the amplitudes and frequencies of spontaneous miniature events. Some spontaneous events were gigantic (10-40 mV), multi-quantal events. Gigantic spontaneous events were eliminated by application of TTX – or by lowered or chelated Ca^{2+} – suggesting that giant events were elicited by spontaneous presynaptic firing. Interestingly, gain-of-function electrophysiological phenotypes were markedly lessened after genetic knockdown or mutation of Drosophila homologs of phospholipase Cβ (PLCβ), IP_3 receptor, or ryanodine receptor (RyR) – all factors known to mediate Ca^{2+} release from intracellular stores. Pharmacological inhibition of intracellular Ca^{2+} store release produced similar effects. Our data suggest inhibition of intracellular Ca^{2+} signaling could counteract hyperexcitability induced by gain-of-function $Ca_V2.1$ amino-acid substitutions.

AUTHOR SUMMARY

Prior research has demonstrated that gain-of-function mutations in a gene important for neurotransmission are known to cause migraine in humans. We attempted to mimic some of those gain-of-function mutations in a simple genetic model organism and examine neurotransmission by electrophysiology. Our findings yield potential clues as to how particular mutations may impact neurophysiology on a cellular level. We used the fruit fly *Drosophila melanogaster* and its model synapse, the neuromuscular junction (NMJ) to perform our studies. Here we document three main

advances: 1) characterization of fruit fly models harboring gain-of-function calcium channel alterations known to cause human familial hemiplegic migraine type 1 (FHM1); 2) characterization of hyperactive neurotransmission caused by one of these alterations; and 3) an ability to quell hyperactive neurotransmission by impairing intracellular Ca^{2+} store release, though both genetic and pharmacological means. Our work contributes to a broader understanding of how pathological mutations could impact cellular physiology. More generally, the utilization of genetic model organisms promises to uncover potential ways to reverse those impacts.

INTRODUCTION

Episodic neurological disorders like migraine, epilepsy, and ataxia can result from underlying ion channel dysfunctions. (1-3). For many such disorders, little is known about how aberrant channel functions affect neuronal signaling paradigms. Cell-based and model organism-based examinations of disease-causing mutations could offer insights into disease-relevant biological processes.

One Mendelian form of migraine – familial hemiplegic migraine type 1 (FHM1) – results from gain-of-function missense mutations in human *CACNA1A*, which encodes the α1 subunit of $Ca_V2.1$ (P/Q)-type calcium channels (4). Two FHM1-causing amino-acid substitutions alter highly conserved $Ca_V2.1$ α1 amino-acid residues, R192 and S218 (4, 5). The R192Q amino-acid substitution (RQ) causes "pure" FHM1, while the S218L substitution (SL) causes a severe combination of FHM1, seizures, and susceptibility to edema following head injury (4, 5). These two FHM1-causing amino-acid substitutions have been studied intensely (6), most notably in knock-in mouse models of FHM1 (7-9).

We have some information about how FHM1 mutant channels impact synaptic machinery to generate dysfunction. FHM1 knock-in mice display gain-of-function $Ca_V2.1$ phenotypes at neurons and synapses. Model synapses studied include those at the diaphragm neuromuscular junction (NMJ) (10, 11), the calyx of Held (12-14), the trigeminal sensory neuron pathway (15-17), and cortical neurons (18, 19). At the mouse NMJ, both RQ and SL increase the frequency of spontaneous excitatory potentials (10, 11). These increases in quantal frequency are dependent on mutation dose and are more

pronounced in SL versus RQ. SL also elicits broadening of evoked end-plate potentials at the mouse NMJ (11). At the mouse calyx of Held, both substitutions result in enhanced excitatory postsynaptic currents (EPSCs) (12-14), and it has been reported that SL causes an increase in the resting intracellular neuronal calcium, which could be responsible for some potentiation of synapse function (12).

It was recently reported that tert-butyl dihydroquinone (BHQ) reverses aspects of SL-induced gating dysfunction and short-term plasticity (20). For part of that study, we demonstrated that BHQ also restores short-term synaptic plasticity to NMJs in fruit fly larvae expressing a transgene that encodes an S161L amino-acid substitution in Drosophila Ca_V2/Cacophony – the functional equivalent of human $Ca_V2.1$ S218L (20). Independent follow-up work by others demonstrated that BHQ application also blunts cortical spreading depression (CSD) susceptibility in mouse S218L (21). Given these results, a further examination of fruit fly synapses could be valuable for uncovering basic molecular and electrophysiological consequences of $Ca_V2.1$ gains of function.

For the present study, we characterized the fruit fly as a way to model neuronal effects of FHM1-causing mutations. We neuronally expressed *cacophony* transgenes harboring the *Drosophila melanogaster* equivalents of RQ or SL – or both RQ and SL concurrently (denoted as "DM" for "double mutant"). On the organismal level, neuronal expression of SL or DM transgenes drastically impaired overall health. Not surprisingly, SL and DM transgenes also markedly enhanced aspects of evoked and spontaneous neurotransmission, consistent with prior studies in mice. Through a combination of genetics, RNA interference, pharmacology, and electrophysiology, we uncovered evidence that a canonical intracellular Ca^{2+} signaling pathway influences levels of neurotransmission and hyperexcitability in the context of gain-of-function Drosophila Ca_V2.

RESULTS

Transgenic Drosophila Ca_V2 "FHM1" channels cause coarse larval phenotypes and fly lethality

We undertook a reverse-translational approach in *Drosophila melanogaster* to study the impact that FHM1-inducing $Ca_V2.1$ amino-acid substitutions may exert on the level of individual synapses. Drosophila *cacophony* encodes the $\alpha1$ subunit of all fruit fly Ca_V2-type channels. We cloned two amino-

acid substitutions that cause human FHM1 (S218L and R192Q) into the analogous codons of a functional Drosophila *UAS-cacophony (cac)-eGFP* transgene (22). Single mutant transgenes are herein termed "SL" (*UAS-cac-eGFP*^{S161L}) (20) or "RQ" (*UAS-cac-eGFP*^{R135Q}) (Fig. 1A). We also generated a double mutant transgene containing both mutations on the same cDNA clone, termed "DM" (*UAS-cac-eGFP*$^{R135Q, S161L}$). "WT" signifies previously characterized wild-type *UAS-cac-eGFP*^{WT} transgenes (22).

We expressed WT, DM, SL, and RQ *UAS-cac-eGFP* transgenes in post-mitotic Drosophila neurons using the *elaV(C155)-Gal4* driver and the *Gal4/UAS* expression system (23, 24). Initially, we examined transgenic animals for visible phenotypes. Neuronal expression of either SL or DM caused larvae to move in a jerky, uncoordinated manner. At the early third instar stage, SL- and DM-expressing animals developed protruding, anterior spiracles prematurely – well before the normal time point of wandering third instar stage and pupation (Fig 1B). Our initial observations also indicated that SL- and DM-expressing animals were not present in expected Mendelian proportions, so we decided to quantify this potential viability phenotype.

We quantified viability of transgenic animals by setting up test crosses and counting adult progeny. For each transgene (WT, DM, SL, and RQ), we set up test crosses (*elaV(C155)-Gal4* females x *Balancer Chromosome*/*UAS-cac-eGFP* males) and counted the number of transgenic *UAS-cac-GFP*-expressing adult progeny and the number of sibling flies carrying a balancer chromosome. We also set up a *Gal4* and balancer chromosome control cross lacking any *UAS-cac-eGFP* transgenes (Table 1). Compared to animals expressing the WT transgene, viability was dramatically diminished for animals expressing the SL and DM transgenes. It was also dramatically diminished for SL- and DM-expressing animals compared to genetically matched siblings carrying the *elaV(C155)-Gal4* driver and a balancer chromosome (Fig. 1C, Table 1). By contrast, WT- and RQ-expressing animals did not show significant defects in viability or statistical differences from the Gal4 control cross. As expected *a priori*, there was a some depressed viability in animals carrying a balancer chromosome. (Fig. 1C, Table 1).

Table 1. Test Crosses and Survival of Adult Progeny.

elaV(C155)-Gal4* x *Balancer /&	*GAL4/+; &/+* progeny (female)	*GAL4/+; Balancer/+* progeny (female)	Normalized Viability Index for & (female)	*GAL4/Y; &/+* progeny (male)	*GAL4/Y; Balancer/+* progeny (male)	Normalized Viability Index for & (male)
& = +	52 (30.6%)	37 (21.8%)	85.1	53 (31.2%)	28 (16.5%)	114.6
& = *UAS-cac^{WT}-GFP*	190 (30.3%)	115 (18.3%)	100.0	205 (32.6%)	118 (18.8%)	105.2
& = *UAS-cac^{DM}-GFP*	**132 (12.7%)*** **	**499 (48.0%)**	**16.0**	**38 (3.7%)*** ###**	**371 (35.7%)**	**6.2**
& = *UAS-cac^{SL}-GFP*	**38 (12.3%)*** **	**136 (44.2%)**	**16.9**	**17 (5.5%)*** #**	**117 (38.0%)**	**8.8**
& = *UAS-cac^{RQ}-GFP*	157 (29.0%)	128 (23.6%)	74.2	147 (27.1%)	110 (20.3%)	80.9

Crosses were performed utilizing *elaV(C155)-Gal4* virgin females x *w/Y; Balancer/ (UAS-cac-GFP or +)* males. Male and female progeny were counted separately. As expected for fruit fly balancer chromosomes, there was lethality associated with inheriting a balancer chromosome. Separately, there was profound lethality associated with inheriting either the *UAS-cac^{DM}-GFP* or *UAS-cac^{SL}-GFP* transgenes driven by pan-neuronal *elaV(C155)-Gal4*. & - denotes the chromosome utilized opposite the balancer in males in the test cross. Normalized Viability Index scores were all calculated starting with the non-Balancer : Balancer progeny ratio; this value was then normalized against the female progeny ratio for the cross where & = *UAS-cac^{WT}-GFP* – i.e., 190/115 = a normalized baseline value of 100.0. For statistical analyses, raw progeny counts were used. *** $p < 0.001$ by Fisher's exact test, compared to gender-matched progeny counts, utilizing the *UAS-cac^{WT}-GFP* as the control. ### $p < 0.001$, # $p = 0.05$, comparing DM- and SL- expressing males vs. DM- and SL-expressing females respectively.

Sex or gene dose of the SL and DM transgenes could influence viability. In Drosophila, X-linked dosage compensation equalizes the expression of X-linked genes by doubling X-linked gene transcription in males (25-27). The X-linked neuronal enhancer trap Gal4 line *elaV(C155)-Gal4* should be expressed at higher levels in hemizygous *elaV(C155)-Gal4/Y* males than in heterozygous *elaV(C155)-Gal4*/+ females. Thus, effects of driving *UAS* transgenes could be stronger in males. Counting male vs. female progeny of SL- and DM-expressing flies revealed that while viability was starkly diminished for both sexes, it was also significantly lower in SL- and DM-expressing males than in SL- and DM-expressing females (Fig. 1C, Table 1).

Finally, we assessed adult fly longevity, comparing WT and DM transgenic flies (Figs. 1D, E). For females, transgenic WT (mean survival: 63 days, *n* = 23) and driver control *elaV(C155)-Gal4/+* animals (66 days, *n* = 16) did not differ with respect to survival. Transgenic DM females (22.5 days, *n* = 28) had severely stunted longevity (Fig. 1D; $p < 0.0001$, Log-rank test). The results for males were consistent: longevity of transgenic WT males (median survival: 56 days, *n* = 38) and driver control *elaV(C155)-Gal4/Y* animals (54.5 days, *n* = 22) did not differ statistically. By contrast, the survival of transgenic DM males (14.5 days, *n* = 10) was markedly diminished (Fig. 1E; $p < 0.0001$, Log-rank test).

Cac-GFP expression levels are comparable across transgenic constructs and Cac-GFP localizes to synaptic active zones

We investigated why SL- and DM-expressing animals were showing diminished viability. We considered the possibility that excessive quantities of α1 protein generated via the *GAL4/UAS* expression system could reduce viability. However, prior studies showed that neuronal overexpression of the WT *UAS-cac-eGFP* transgene renders no discernible structural, behavioral, or electrophysiological abnormalities. Additionally, overexpressed Cac-GFP protein efficiently localizes to active zone structures at synapses like the larval neuromuscular junction (NMJ) (20, 22, 28-31).

We assessed whether differential expression or localization of each *UAS-cac-eGFP* could underlie observed reductions in viability. Using wandering third instar larvae, we quantified and compared levels of *elaV(C155)-Gal4*-driven transgene expression for transgenic lines: WT (published line - *UAS-cac-eGFP*^{786c}) (22), RQ (*UAS-cac-eGFP*$^{R/Q(1M)}$) (this study), SL (*UAS-cac-eGFP*$^{S/L(3\text{-}2M)}$) (20), and DM (*UAS-cac-eGFP*$^{DM(2M)}$) (this study). We used an anti-GFP antibody to detect Cac-GFP and co-stained with a monoclonal antibody against the presynaptic ELKS/CAST active zone protein Bruchpilot (Brp) (32) in the central nervous system and synaptic structures. We then quantified Cac-GFP staining levels and intensity by immunofluorescence microscopy. In the central nervous system, we found no significant differences in Cac-GFP protein intensity regardless of genotype or transgene insertion (Figs. 2A-E, Red channel). We next considered Cac-GFP localization at the NMJ. We found that all WT and mutant transgenic Cac-GFP proteins successfully localized to synaptic active zones as previously

reported for the original WT constructs (22, 28). By co-staining with anti-Brp and anti-GFP, we observed significant Cac-GFP protein at Brp-positive NMJ active zones for all chosen transgenic lines (Fig. 2F-I).

DM-expressing NMJs show small changes in bouton number and glutamate receptor density

Transgenic mutant Cac-GFP expression could potentially affect synapse growth or development. We previously found no abnormalities in NMJ synaptic growth for SL-expressing flies (20). For this study, we extended our analysis for the DM transgene line by co-staining third instar larval NMJs with antibodies against the Drosophila PSD-95 homolog, Discs Large (Dlg) and the GluRIIA glutamate receptor subunit. We observed a small numerical decrease in the number of Dlg-positive synaptic boutons at DM-expressing NMJs compared to control WT-expressing NMJs. This small decrease was statistically significant only for segment A2, muscle 6/7 (Fig. 2J). Additionally, we found no significant change in the number of glutamate receptor clusters per NMJ comparing WT-expressing synapses and DM-expressing synapses (Fig. 2K).

At DM-expressing NMJs, the percentage of the synaptic area covered by the GluRIIA clusters – normalized to total Dlg area – was slightly but significantly increased (Fig. 2L). Moreover, we also observed a very small (~ 7%), but statistically significant increase in the average intensity of GluRIIA-containing glutamate receptor clusters, normalized to Dlg intensity (Fig. 2M) – while average Dlg intensity itself was unchanged between WT- and DM-expressing NMJs. In principle, an expansion of the synaptic area capable of receiving neurotransmitter and a slightly denser packing of GluRIIA-containing receptors could yield gains in synaptic transmission (33). However, the magnitude of any such change based on this postsynaptic staining profile alone (< 10% increase in receptor density) would likely be small or nonexistent. We elected to conduct finer analyses by electrophysiology.

DM-, SL- and RQ-expressing NMJs display hyperexcitable evoked synaptic discharges

Coarse phenotypes from neuronally expressed DM and SL transgenes (Fig. 1) suggested abnormal neuronal or synapse function. We turned to NMJ electrophysiology to document possible synaptic dysfunctions caused by the mutant transgenes. We hypothesized that the neuronal expression

of gain-of-function *UAS-cac-GFP* transgenes could result in enhanced evoked NMJ neurotransmission in Drosophila, similar to the knock-in mouse FHM1 models.

Expression of both SL and DM significantly increased EPSP amplitudes across a range of low extracellular [Ca^{2+}] (0.2–0.5 mM) (Fig. 3A, 3D; data for 0.4 mM $[Ca^{2+}]_e$ are shown) (20). Expression of RQ also increased average NMJ EPSP amplitudes, but this increase was not statistically significant (Fig. 3A). Interestingly, neither calculated quantal content (QC) (Fig. 3B) nor calcium cooperativity of release for mutant lines were significantly different than WT across this range of 0.2–0.5 mM [Ca^{2+}] (Fig. 3C) (20) (but see more detailed quantal analyses later).

In the course of collecting evoked neurotransmission data, we noted that the EPSP waveforms of RQ, SL, and DM animals were sometimes abnormal (compare Figs 3D, E). Specifically, we observed two distinct phenotypes: 1) 'extra discharges' ("ED"), in which supernumerary spiking events occurred during the decay phase of the EPSP waveform (Fig. 3E, left); and 2) 'shoulders,' in which there was an extended discharge during the decay phase of the EPSP (Fig. 3E, right), causing a discontinuity in the decay. These phenotypes were somewhat reminiscent of a broadening of the end-plate potential previously reported at the NMJs of SL knock-in mice (11). The SL-expressing NMJs produced only the extra discharge type of abnormal waveform, whereas the RQ-expressing NMJs produced only the shoulder form (Figs. 3E, F). Consistent with both mutations being present in DM, those NMJs exhibited both types of abnormal waveform (Fig. 3F). Finally, we generated "RQ only" animals – null cac^{HC129} mutant larvae rescued to viability by expression of the RQ transgene (we were unable to generate similar "SL only" or "DM only" animals, likely due to deleterious gains of function from the SL mutation). In the case of "RQ only", the waveform dysfunction closely matched that shown by the RQ-expressing NMJs (Fig. 3F) – i.e. a shoulder waveform phenotype was present.

Next, for the SL- and DM-expressing animals, we assessed the severity of the extra discharge phenotype by counting the number of extra discharge events per 30 evoked pulses (30 recording sweeps at 1 Hz per NMJ). Quantification confirmed that SL- and DM-expressing NMJs were highly dysfunctional, possibly due to underlying neuronal hyperexcitability (Fig. 3G). A previous study in Drosophila demonstrated that magnesium in the recording saline can mask defects in the excitability of

234 neurons (34). Therefore, we extended our analyses by conducting additional WT and DM recordings in
235 saline with lowered $MgCl_2$ (6 mM vs. 10 mM for normal saline). DM-expressing NMJs displayed extreme
236 dysfunction in 6 mM $MgCl_2$, both in terms of the percentage of NMJs that produced supernumerary
237 discharges (100%, Fig. 3H) and the number of extra discharges counted per 30 presynaptic pulses (Fig.
238 3I). By contrast, WT-expressing NMJs showed no significant dysfunction (Figs. 3H, I). In all, SL- and DM-
239 expressing NMJs displayed evoked gain-of-function phenotypes consistent with prior mammalian FHM1
240 mutant analyses.
241
242 **SL- and DM-expressing NMJs show enhanced spontaneous miniature EPSPs with respect to both**
243 **amplitude and frequency**
244 The evoked neurotransmission data indicated synapse hyperexcitability in the mutant transgenic
245 flies. Mammalian models of FHM1 also show dysfunctional spontaneous neurotransmission (10, 11).
246 Therefore, we extended our electrophysiological analyses to quantal neurotransmission. We observed a
247 striking phenotype: for SL- and DM-expressing NMJs, there was a significant enhancement in both
248 amplitude and frequency of spontaneous miniature EPSPs (mEPSPs) (Figs. 4A-C, Table 2). By contrast,
249 neither an increase in spontaneous mEPSP amplitude nor mEPSP frequency were observed for RQ- or
250 WT-expressing NMJs compared to non-transgenic w^{1118} controls (Figs. 4B-E, Table 2). Interestingly, we
251 also noted that the spontaneous events at SL- and DM-expressing NMJs also included a small minority
252 of gigantic spontaneous events (10-40 mV) that were never seen in controls or RQ-expressing NMJs
253 (Figs. 4A, D, E). These gigantic events were seen in the complete absence of presynaptic nerve
254 stimulation in nerves that had already been severed from the central nervous system. Follow-up
255 analyses of thousands of individual spontaneous events per genotype revealed that increases in
256 spontaneous amplitudes were due to an overall increase in the size distribution of the events at SL- and
257 DM-expressing NMJs (Figs. 4D, E), which also included the rare gigantic events, never observed at
258 w^{1118}, WT-, or RQ-expressing NMJs (Fig. 4D).
259 **Table 2. Raw electrophysiological data of spontaneous (mEPSP) events – Ca^{2+} and Na_V.**

Line	Saline	n	Average mEPSP (mV)	mEPSP Freq (Hz)	Median mEPSP (mV)	Maximum mEPSP (mV)	Resting Membrane V (mV)	Analysis Figures
w^{1118}	0.5 mM $[Ca^{2+}]$	13	0.86 ± 0.07	4.6 ± 0.4	0.69	11.53	-62.9 ± 0.9	4, 5
GAL4 > WT		17	0.77 ± 0.05	2.8 ± 0.2	0.67	7.24	-67.8 ± 0.9	4, 5, 6
GAL4 > DM		25	1.75 ± 0.22	5.8 ± 0.7	1.04	36.91	-68.2 ± 1.2	4, 5, 6
GAL4 > SL		12	1.32 ± 0.16	6.7 ± 1.0	0.76	44.42	-65.4 ± 0.9	4, 5, 6
GAL4 > RQ		13	0.77 ± 0.05	3.4 ± 0.4	0.61	3.88	-64.7 ± 1.0	4, 5
w^{1118}	0.4 mM $[Ca^{2+}]$	15	0.70 ± 0.03	3.7 ± 0.2	0.61	3.37	-61.4 ± 0.4	3
GAL4 > WT		25	0.79 ± 0.05	3.1 ± 0.2	0.66	5.41	-64.2 ± 0.9	3
GAL4 > DM		17	1.48 ± 0.13	6.0 ± 0.7	1.10	41.17	-62.2 ± 0.6	3
GAL4 > SL		14	1.66 ± 0.19	6.6 ± 1.1	1.18	57.90	-65.1 ± 1.6	3
GAL4 > RQ		12	0.79 ± 0.06	4.3 ± 0.4	0.69	3.38	-66.5 ± 1.7	3
w^{1118}	0.2 mM $[Ca^{2+}]$	9	0.64 ± 0.03	3.9 ± 0.3	0.56	2.73	-61.2 ± 0.9	5
GAL4 > WT		12	0.70 ± 0.06	2.5 ± 0.3	0.59	2.88	-67.1 ± 1.3	5
GAL4 > DM		19	1.34 ± 0.08	5.2 ± 0.6	1.11	19.95	-61.8 ± 0.9	5
GAL4 > SL		14	0.94 ± 0.08	7.0 ± 1.1	0.77	5.93	-65.6 ± 1.6	5
GAL4 > RQ		8	0.77 ± 0.04	2.0 ± 0.4	0.66	2.88	-58.7 ± 0.5	5
GAL4 > WT	0 mM $[Ca^{2+}]$	9	0.73 ± 0.05	2.7 ± 0.3	0.61	3.31	-60.1 ± 1.4	5
GAL4 > DM		10	1.15 ± 0.09	8.4 ± 1.6	0.98	6.59	-58.0 ± 1.6	5
GAL4 > SL		11	1.17 ± 0.11	12.6 ± 2.3	0.93	5.42	-58.7 ± 0.6	5
GAL4 > WT	BAPTA-AM and TTX controls	18	0.73 ± 0.02	4.2 ± 0.4	0.65	3.04	-66.5 ± 1.2	5
GAL4 > DM		16	1.29 ± 0.14	7.4 ± 0.7	0.92	41.56	-64.4 ± 0.8	5
GAL4 > WT	+ 10 μM BAPTA-AM	9	0.62 ± 0.06	1.6 ± 0.2	0.51	3.67	-60.4 ± 1.9	5
GAL4 > DM		8	1.16 ± 0.10	2.0 ± 0.2	0.97	5.50	-59.5 ± 1.0	5
GAL4 > WT	+ 3 μM TTX	7	0.66 ± 0.05	3.8 ± 0.4	0.54	2.82	-62.1 ± 1.1	5
GAL4 > DM		18	1.09 ± 0.07	6.9 ± 0.7	0.85	9.82	-62.5 ± 0.7	5

Average mEPSP amplitudes ± SEM and mEPSP frequencies ± SEM for selected conditions. Also given: median mEPSP amplitudes and maximum mEPSP amplitudes achieved for spontaneous events analyzed (~100 per NMJ). w^{1118} is a non-transgenic wild-type control. WT, DM, SL, and RQ are shorthand for the indicated *UAS-cac-eGFP* transgene being driven in male progeny presynaptically by the *elaV(C155)-GAL4* driver. These data illustrate differential effects when lowering extracellular $[Ca^{2+}]$, chelating Ca^{2+} with BAPTA-AM, or inactivating Na_V channels with TTX.

We checked if acute *cac* transgene expression was sufficient to cause spontaneous neurotransmission phenotypes. We utilized the temperature-sensitive *Gal80^{TS}/TARGET* system to temporally control expression of the DM transgene (35). To conduct this experiment, we generated *elaV(C155)-Gal4 >> UAS-cac^{DM}* animals with a ubiquitous *Gal80^{TS}* transgene (35). Gal80^{TS} protein halts

Gal4-induced gene expression at permissive temperatures (25ºC) but not at restrictive temperatures (29ºC). For our experiment, animals raised at 25ºC throughout life had no discernible spontaneous neurotransmission hyperexcitability (Fig. 4F). By contrast, animals started at 25ºC and shifted to 29ºC for the final 24 or 48 hours before third instar NMJ recording showed progressively more spontaneous hyperexcitability (Figs. 4F, G).

Gigantic spontaneous events require extracellular calcium and sodium channel activity

Prior work proposed that mammalian neuronal dysfunction downstream of FHM1 mutations may be calcium-dependent (12). We tested whether the observed effects on quantal size in our model could be calcium-dependent. First, we reduced the extracellular [Ca^{2+}] in the recording saline from 0.5 mM to 0.2 mM. Consistent with classic characterizations of Drosophila NMJ properties (36), low calcium did little to change the distribution of mEPSP size, the median mEPSP size, or the 25^{th}-75^{th} percentiles of mEPSP size – all of which remained normal for WT and elevated for SL- and DM-expressing NMJs (Figs. 5A, B, Table 2). However, lowering extracellular [Ca^{2+}] almost completely abrogated gigantic (10-40 mV) spontaneous events at SL- and DM-expressing NMJs – and it completely eliminated the very largest ones (Figs. 5A, B). This suggested that these gigantic events somehow relied on a sufficient driving force of presynaptic calcium influx – and potentially on spontaneous presynaptic nerve firing.

We extended these analyses by altering the recording saline in three additional ways: 1) zero extracellular calcium; 2) adding the membrane-permeable calcium chelator, 1,2-Bis (2-aminophenoxy) ethane-N,N,N′,N′-tetra acetic acid tetrakis (acetoxymethyl ester) (BAPTA-AM, 10 μM); or 3) adding tetrodotoxin (TTX, 3 μM) to block voltage-gated sodium channels. We compared WT-expressing and DM-expressing NMJs (and SL-expressing NMJs in the case of zero calcium). All three manipulations produced a similar effect on mEPSP size for the gain-of-function mutants: an elimination of gigantic spontaneous events, but a persistence of overall elevated mEPSP size (Figs. 5C-F, Table 2). By contrast, these manipulations had minimal to no effect on the distribution of mEPSP amplitudes at WT-expressing NMJs (Figs. 5C-D, Table 2).

Large spontaneous events are due to multi-vesicular release

The presence of gigantic spontaneous mEPSPs that were sensitive to low calcium, calcium chelation, and TTX treatment suggested the possibility of spontaneous multi-vesicular release at SL- and DM-expressing NMJs. If this were true, traditional analysis of spontaneous mEPSPs would result in an overestimation of average quantal size (Fig. 4B) and underestimation of average QC (Fig. 3B) for SL- and DM-expressing NMJs.

We utilized the method of failures to better resolve questions about quantal size and QC. At very low concentrations of extracellular calcium, synapses like the NMJ are essentially limited to a one-or-none evoked response in which stimulation of the presynaptic nerve either leads to the release of a single vesicle or fails to release any vesicles (37). By conducting failure analyses, it is possible to measure the distribution of quantal events and also to estimate QC in a way that eliminates confounds of higher concentrations of calcium. First, we conducted failure analysis recordings at 0.14 mM $[Ca^{2+}]_e$ for WT-, DM-, and SL-expressing NMJs (Figs. 6A-C). For this condition, the evoked events for SL- and DM-expressing NMJs were far larger on average than those observed WT-expressing NMJs (Fig. 6C – EPSP). This was due to a large proportion of events of > 2 mV for the SL- and DM-expressing conditions (compare Figs. 6A, B for WT vs. DM). Furthermore, even in this low level of extracellular Ca^{2+}, many of DM and SL events represented multi-vesicular release rather than the release of a single large vesicle. We calculated values of QC of > 2 for both mutant conditions at 0.14 mM $[Ca^{2+}]_e$ (QC = m = ln[(# trials)/(# failures)] (38)) (Fig. 6C).

To test if lower calcium could generate a leftward shift in event size, we applied a more restrictive condition of 0.1 mM $[Ca^{2+}]_e$ to DM-expressing NMJs. At 0.1 mM $[Ca^{2+}]_e$ the proportion of failures was very high for DM-expressing NMJs, with events over 4 mV all but absent, and events greater than 1.5 mV also less prevalent (Fig. 6C). The first peak in the distribution of events, which is reflective of single vesicle size (38), was centered near 0.7 mV, a value consistent with single-vesicle responses of normal size for the Drosophila NMJ (36). Together, these data suggested that the observed large events at SL- and DM-expressing NMJs – regardless of whether spontaneous or failure analysis-evoked – were likely due to multi-vesicular release (see Fig. 6E, spontaneous and failure analyses distributions side-by-side).

326

327 **PLCβ loss genetically suppresses spontaneous excitability**

328 For SL- and DM-expressing NMJs, we hypothesized that specific cellular cues could dictate the
329 various electrophysiological phenotypes we documented: multi-vesicular quantal events, gigantic TTX-
330 sensitive spontaneous events, and enhanced NMJ excitability. We inquired as to what the molecular
331 nature of those cues might be. Our experiments indicated that intracellular calcium or intracellular
332 calcium signaling processes might be important (Fig. 5). Additionally, recent data from the mouse calyx
333 of Held demonstrated that S218L knock-in synapses have enhanced resting intracellular calcium (12).
334 We hypothesized that altered intracellular calcium signaling or handling could impact myriad intracellular
335 signals and investigated which signaling pathways might be relevant.

336 This line of inquiry spurred a directed genetic approach examining regulators of intracellular
337 calcium release to test if inhibition of any of these factors may influence gain-of-function Ca_V2
338 phenotypes at the synapse (Fig. 7A). We sought to identify suppressors capable of reversing gains of
339 Ca_V2 function caused by the SL and DM transgenes.

340 Prior studies of Drosophila NMJ presynaptic homeostatic potentiation – which involves the
341 potentiation of Ca_V2 – suggested some possible candidate molecules (39, 40). Additionally, we
342 previously showed that the Drosophila PLCβ homolog *phospholipase-C at 21C* (*Plc21C*) is necessary for
343 the neuronal homeostatic potentiation mechanism (41). Plc21C is one of two Drosophila Phospholipase-
344 Cβ (PLCβ) family members, and is expressed in the nervous system (42). Canonically, PLCβ proteins
345 cleave phosphatidylinositol 4,5-bisphosphate (PIP_2) to generate soluble inositol triphosphate (IP_3), as
346 well as membrane-bound diacylglycerol (DAG). These signaling factors influence synaptic transmission
347 in a variety of ways, including direct modulation of Ca_V2 (43), and they have been shown to act at several
348 synapses, including the NMJ (44-49).

349 We targeted *Plc21C* gene expression in neurons with a previously verified *UAS-Plc21C(RNAi)*
350 construct, $Plc21C^{GD11359}$ (41, 50). Compared to the NMJs of w^{1118} and WT controls, those in which only
351 *Plc21C* had been knocked down presynaptically exhibited no discernable baseline changes in mEPSP
352 size (Fig. 7B, Table 3) – or as previously documented, EPSP size, or QC (41). By contrast, in DM-

353 expressing NMJs such *Plc21C* knockdown alleviated aspects of NMJ hyperexcitability. Specifically, there
354 was a leftward shift in the distribution of spontaneous events (Fig. 7B, Table 3).

355

356 **Table 3. Raw electrophysiological data of spontaneous (mEPSP) events – impairment of**
357 **intracellular Ca^{2+} handling pathway.**

Line	Experiment (all 0.5 mM Ca^{2+})	n	Average mEPSP (mV)	mEPSP Freq (Hz)	Median mEPSP (mV)	Maximum mEPSP (mV)	Resting Membrane V (mV)	Analysis Figures
w^{1118} females	*Plc21C* RNAi baseline	27	0.81 ± 0.05	4.3 ± 0.3	0.64	7.16	-62.2 ± 0.6	7
Plc21C(RNAi) males		12	0.80 ± 0.06	2.0 ± 0.2	0.61	4.50	-66.5 ± 0.9	N/A
Plc21C(RNAi) females		6	0.83 ± 0.02	3.8 ± 0.9	0.59	7.68	-61.6 ± 0.3	7
GAL4 > DM females	suppression of DM	19	1.28 ± 0.08	5.8 ± 0.5	1.01	7.62	-67.0 ± 1.2	7
GAL4 > DM + Plc21C(RNAi) females		13	0.78 ± 0.04	5.2 ± 0.6	0.68	3.89	-64.9 ± 1.6	7
GAL4; $itpr^{ug3}$/+	suppression of *DM*	9	0.74 ± 0.04	3.7 ± 0.2	0.64	3.34	-61.3 ± 0.6	7
GAL4 > DM; $itpr^{ug3}$/+		14	1.05 ± 0.06	6.1 ± 0.5	0.86	16.21	-65.8 ± 0.7	7
GAL4; RyR^{E4340K}/+	suppression of *DM*	13	0.83 ± 0.03	3.3 ± 0.3	0.70	3.38	-63.0 ± 0.5	7
GAL4 > DM; RyR^{E4340K}/+		17	0.91 ± 0.04	5.1 ± 0.8	0.76	5.13	-62.5 ± 0.9	7
GAL4 > WT	XestC and LiCl controls	19	0.80 ± 0.02	2.3 ± 0.3	0.71	2.59	-69.6 ± 1.1	8
GAL4 > DM		30	1.63 ± 0.13	6.6 ± 0.7	1.08	51.03	-65.8 ± 0.7	8
GAL4 > WT	+ 5 µM XestC	7	1.04 ± 0.04	3.5 ± 0.9	0.78	3.80	-69.8 ± 2.2	8
GAL4 > DM		14	1.14 ± 0.11	6.4 ± 1.1	0.81	30.76	-67.2 ± 1.3	8
GAL4 > WT	+ 10 mM LiCl	11	0.81 ± 0.03	3.2 ± 0.4	0.73	4.09	-66.6 ± 1.3	8
GAL4 > DM		12	1.2 ± 0.06	4.1 ± 0.4	0.98	6.34	-68.8 ± 1.7	8

358

359 Average mEPSP amplitudes ± SEM and mEPSP frequencies ± SEM for selected
360 experimental conditions. Also given are the median mEPSP amplitude and the maximum
361 mEPSP amplitudes achieved for all spontaneous events analyzed per genotype (~100 per

NMJ). w^{1118} is a non-transgenic wild-type control. WT and DM are shorthand for the indicated *UAS-cac-eGFP* transgene being driven in progeny presynaptically by the *elaV(C155)-GAL4* driver. This table illustrates differential effects when impairing an intracellular calcium handling pathway through mutation of the *Plc21C*, *itpr*, and *RyR* genes, or through pharmacological application of Xestospongin C or LiCl.

IP_3R and RyR point mutations strongly suppress hyperexcitability

We hypothesized that Plc21C could exert effects on spontaneous neurotransmission via one of several components of its canonical signaling pathway (e.g. PIP_2, DAG, or IP_3). Notably, IP_3 acts through the IP_3 receptor (IP_3R), an intracellular calcium channel located on the endoplasmic reticulum (ER). At other model synapses, release of Ca^{2+} from the intracellular stores can promote the release of neurotransmitter-laden vesicles and contribute to the amplitudes of spontaneous events (51-54). Moreover, IP_3R has been proposed to play a role in spontaneous vesicle release through calcium-induced calcium release (CICR) (55), and increased ER Ca^{2+} release was recently shown to potentiate synaptic transmission at the Drosophila NMJ (56).

We examined the Drosophila IP_3R gene (*itpr*). Homozygous *itpr* mutations are lethal, so we first tested a heterozygous loss-of-function condition. Since IP_3R clusters consist of multiple units, we hypothesized that we might be able to disrupt them through a loss-of-function point mutation, $itpr^{\mu g3}$, a mutant possessing a missense mutation in the IP_3R ligand-binding domain (57). $itpr^{\mu g3}$/+ phenocopied *Plc21C* knockdown at DM-expressing NMJs: the mEPSP amplitude was partially reduced toward WT levels, and the number of giant, spontaneous events was diminished (Figs. 7C, D, Table 3). Importantly, on its own $itpr^{\mu g3}$/+ did not significantly affect the baseline amplitude or distribution of mEPSPs (Fig. 7C, Table 3).

We performed analogous experiments with a Drosophila ryanodine receptor gene (*RyR*) mutation. Tetrameric RyR channels have been reported to contribute to CICR downstream of IP_3Rs (55). Additionally, gigantic spontaneous miniature potentials at other model synapses are mediated by RyR and rapid expulsion of calcium from presynaptic stores (58-62). We found that the heterozygous *RyR* point mutant RyR^{E4340K}/+ (63) almost completely suppressed the DM mEPSP phenotype. The increased average mEPSP in the DM-expressing background was suppressed (Figs. 7C, E, Table 3), and the

391 gigantic spontaneous events were abrogated (Figs. 7C, E, Table 3). Control recordings showed that
392 *RyR*^{E4340K}/+ did not affect the baseline amplitude or distribution of mEPSPs (Fig. 7C).

393 Because the *RyR*^{E4340K}/+ background provided such a strong suppression of spontaneous
394 mEPSP hyperexcitability at DM-expressing NMJs, we checked if it could also suppress hyperexcitability
395 in the context of evoked excitation. As shown before, when incubated in low extracellular magnesium,
396 100% of the DM-expressing NMJs showed a hyperexcitability dysfunction, with high expressivity of extra,
397 epileptiform discharges (Figs. 3H,I; 7F). By contrast, in a heterozygous *RyR*^{E4340K}/+ genetic background,
398 this hyperexcitability was somewhat suppressed, in terms of both the penetrance of NMJs with extra
399 evoked discharges and the expressivity of the extra discharge dysfunction at individual NMJs (Fig. 7F).

400

401 **Spontaneous mEPSP hyperexcitability can be suppressed pharmacologically**

402 Our data for genetic manipulations affecting Plc21C, IP_3R, and RyR show that it is possible to
403 attenuate DM-induced gain-of-function mEPSP phenotypes by manipulating factors involved in
404 intracellular Ca^{2+} release. In addition to genetic manipulations, we wondered if chronic or acute
405 pharmacological manipulations could also be effective. We turned to two agents to test this idea: lithium
406 (10mM LiCl in larval food) and Xestospongin C (5 μM in recording saline). Chronic exposure to LiCl
407 inhibits inositol monophosphate phosphatase, eventually resulting in a disruption of the recycling process
408 that generates PIP_2 (64, 65). By contrast, Xestospongin C has been characterized as a membrane-
409 permeable inhibitor of IP_3 receptors (66, 67). Either chronically feeding larvae LiCl or applying
410 Xestospongin C to the recording bath caused a significant leftward shift in the overall size distribution of
411 spontaneous amplitudes (Figs. 8A-C), reminiscent of the effects observed for *Plc21C*, *itpr*, and *RyR*
412 losses of function. The acute Xestospongin C application seemed to exert a stronger suppression effect
413 in this regard, while the chronic LiCl application exerted a stronger suppression of the gigantic
414 spontaneous events (Figs. 8 A-C, Table 3). Notably, neither pharmacological manipulation diminished
415 baseline spontaneous neurotransmission in WT-expressing control NMJs (Figs 8A-C, Table 3).

416

417 **DISCUSSION**

We generated fruit flies designed to mimic the effects of FHM1-inducing $Ca_V2.1$ channel mutants, R192Q and S218L. Flies expressing the SL and DM transgenes for Drosophila Ca_V2/Cacophony displayed overt phenotypes, including reduced viability (Fig. 1). They also displayed synaptic phenotypes, including enhanced evoked excitability (Fig. 3), stark increases in quantal size and frequency (Fig. 4), giant, spontaneous, sodium channel-dependent events (Figs. 4, 5), and enhanced probability of release at very low calcium (Fig. 6). All of these neurotransmission phenotypes occurred without major alterations to synaptic architecture (Fig. 2). By contrast, RQ-expressing NMJs had only a mild phenotype: EPSP discharges with shoulder-like waveforms (Fig. 3). Genetic knockdown of Drosophila PLCβ or mutations affecting the receptors that gate intracellular calcium stores (IP_3 receptor and Ryanodine receptor) partially alleviated some of the electrophysiological phenotypes (Fig. 7), as did pharmacological manipulations targeting the same processes (Fig. 8). These results suggest that intracellular Ca^{2+} signaling through IP_3 receptors and Ryanodine receptors could influence physiological dysfunction in a gain-of-function Ca_V2 background (Fig. 8D). Additionally, given the ability of TTX to block gigantic spontaneous events – and given our ability to quiet that phenotype through genetic and pharmacological means – impairment of the IP_3 Receptor/Ryanodine Receptor pathway may limit spontaneous neuronal firing by as-yet undetermined mechanisms (Fig. 8D).

Similarities between fly mutations and FHM1-causing human mutations

Evoked Neurotransmission. Our discovery that SL- and DM-expressing Drosophila NMJs displayed increased evoked excitation, especially at low $[Ca^{2+}]_e$ (Figs. 3, 6) (20), was consistent with findings from diaphragm NMJs in SL knock-in mice (11). In that context, the end-plate potential (EPP) amplitudes were significantly increased at low levels of calcium (0.2 mM), but did not differ from those at wild-type NMJs at physiological calcium (2 mM) (11). Interestingly, at the SL knock-in calyx of Held, excitatory postsynaptic currents (EPSCs) were increased, but this effect was most pronounced at high levels of $[Ca^{2+}]_e$ (12). The extended or epileptiform EPSP discharges caused by expression of the SL-containing transgenic constructs in flies (Fig. 3) were reminiscent of the EPP broadening at SL knock-in NMJs (11). Finally, the severity of the dysfunction in the Drosophila NMJ waveform in the context of

445 decreased extracellular magnesium (6 mM) (Fig. 3) was consistent with a marked increase in calcium
446 current in response to long action potential waveforms in calyces of Held expressing the RQ or SL
447 mutant protein (12, 14).

448 *Enhanced Quantal Frequency.* The enhanced mEPSP frequency at SL- and DM-expressing
449 Drosophila NMJs (Fig. 4, Table 1) was reminiscent of observations in prior FHM1 studies. In the RQ and
450 SL knock-in mice, the NMJs exhibited significant increases in the frequency of mEPPs (9-11).
451 Theoretically, this spontaneous activity could ultimately lead to a buildup of intracellular calcium or a
452 change in intracellular calcium dynamics. In support of this view, at the calyx of Held in SL knock-in mice
453 the frequency of spontaneous mEPSCs was enhanced and resting $[Ca^{2+}]_i$ was elevated (12). In that
454 case, the increase in quantal frequency was partially reversed by adding the cell-permeable calcium
455 chelator EGTA-AM (12).

456 Evidence from several model synapses suggests that Ca_V2 channels can play a prominent role in
457 spontaneous release. In granule cells of the hippocampus, stochastic activity of $Ca_V2.2$-type channels
458 potentiates spontaneous miniature events, and the application of either BAPTA-AM or EGTA-AM is
459 sufficient to inhibit them (68). Other studies demonstrated that P/Q-, N-, and R-type calcium channels
460 also promote spontaneous release (69). Notably, the differences in the spontaneous miniature
461 phenotype between mice harboring the SL and RQ knock-in substitution, or fruit flies expressing
462 mimicking mutations, suggest that the differences in cellular outcomes occur downstream of the Ca_v2
463 channel. This highlights a need for genetic approaches to uncover pathways that might contribute to the
464 divergent phenotypes, as well those that are shared, to better understand the biology downstream of
465 gain-of-function calcium channel activity.

466

467 **Differences between fly mutations and FHM1-causing human mutations**

468 *Quantal amplitudes.* While FHM1 mutations have been shown to enhance spontaneous miniature
469 quantal release frequency in other systems (8-11), there has been no report of increases in spontaneous
470 miniature quantal size due to these mutations. In theory, an increase in the amplitude of mEPSP events
471 at the Drosophila NMJ could be explained by an alteration to the expression and localization of

472 postsynaptic proteins. Yet immunostaining of postsynaptic markers did not strongly support this
473 possibility (Figs. 2J-M), nor did the results of the temperature shift experiments and transient DM
474 expression (Fig. 4G). Instead, failure analyses pointed to alterations to the nature of spontaneous,
475 presynaptic vesicle release (Fig. 6).

476 Why do SL- and DM-expressing NMJs in Drosophila show an increase in quantal size through
477 multi-vesicular release? The synaptic preparation examined is likely to be critical. Evidence from other
478 systems has demonstrated that calcium-channel activity can have a profound effect on quantal size. For
479 example, work at the *C. elegans* NMJ has demonstrated that calcium from intracellular and extracellular
480 sources combines to dictate quantal size and frequency (52). Additionally, spontaneous miniature events
481 with large amplitudes ("maximinis") have been documented at fast inhibitory synapses of the cerebellum
482 (51, 70). Similar to the NMJ activity documented in our study, these maximinis rely on the ability of
483 ryanodine-sensitive stores to support spontaneous calcium transients large enough to cause multi-
484 vesicular release. It is possible that the architecture of a giant synapse like the Drosophila NMJ – which
485 contains hundreds of active zones clustered into individual boutons and has a low level of spontaneous,
486 multi-vesicular release (71) – makes it exquisitely sensitive to small changes in intracellular calcium
487 handling.

488 *Evoked waveforms*. As is the case for the Drosophila NMJ (Fig. 2), the diaphragm NMJ of FHM1
489 knock-in mice displayed EPP broadening (11). The mouse and fly NMJ models are similar in that evoked
490 dysfunction is enhanced by the elicitation of events by stimuli of long duration (14). However, the extra,
491 epileptiform discharges we find at the Drosophila NMJ do not seem to be documented for the
492 mammalian NMJ. An instructive parallel can be drawn between our data and cultures of Drosophila giant
493 neurons, in which manipulation of the voltage-gated potassium current generated altered waveforms,
494 including extra and extended discharges (72, 73). This raises the possibility that some aspects of the
495 FHM1 phenotypes may be caused by the perturbation of other voltage-activated currents, and by
496 synapse excitability more generally (74). This possibility is also consistent with the fact that mutations in
497 the Na^+/K^+ ATPase gene cause pure FHM (75). Given the effectiveness of the Drosophila system for

uncovering complex homeostatic relationships amongst ion channel activities, in particular potassium currents, the fly may be a good model for studying the cellular bases of disorders such as FHM1 (76-80).

Implications for gain-of-function calcium channel and migraine signaling pathways

One strength of Drosophila is the power of genetic manipulation. In this study, we have shown that the expression of gain-of-function transgenes bearing mutations mimicking those associated with migraine in humans causes overt spontaneous and/or evoked phenotypes. Further, we have shown that impairment of a PLCβ-directed signaling pathway occludes several aspects of spontaneous dysfunction. A simple explanation – but certainly not the only explanation – is that $Ca_V2.1$ gains of function potentiate the activities of the IP_3R and RyR channels (81-84). Our work does not directly show this. However, the implication of PLCβ activity and intracellular calcium handling in hyperexcitability fit with the results of prior migraine studies. One recent RNA profiling analysis of the cerebellum of SL knock-in mice revealed an overrepresentation of several signaling pathway components, including PLCβ (85). Moreover, PLCβ and the release of calcium from intracellular stores have been implicated in signaling by calcitonin gene related peptide (CGRP) (86-88), whose levels are correlated with migraine (89-91). Further investigation will be needed to establish whether there is a causative link between the action of intracellular calcium stores either in inducing migraine or in precipitating neurological events that precede some forms of migraine, like aura and cortical spreading depression.

MATERIALS AND METHODS

Gain-of-function *cacophony* constructs: To generate *UAS-cac-eGFP*^{SL} transgenes, we used PCR to alter the serine 161 codon to leucine in the pUAST-based *UAS-cac-eGFP* DNA construct (20, 22). This substitution corresponds to S218L in mammalian CACNA1A. To generate *UAS-cac-eGFP*^{RQ} transgenes, we used PCR to change the arginine 135 codon to glutamine. This substitution corresponds to R192Q in mammalian CACNA1A. For the *UAS-cac-eGFP*^{DM} transgene, both mutations were incorporated into the same *UAS-cac-eGFP* construct using PCR to link the overlapping RQ and SL fragments. Transgenic

lines were generated by injection of *UAS-cac-eGFP* constructs into a w^{1118} background (The Best Gene, Chino Hills, CA) and mapped and backcrossed.

Drosophila Stocks, Genetics, and Husbandry: Animals used for viability counts and electrophysiology were generated by driving neuronal expression of *UAS-cac-eGFP* transgenes with *elaV(C155)-GAL4* (23). Multiple *UAS-cac-eGFP* transgenic lines were initially examined to control for possible differences caused by independent *UAS* genomic insertions: WT: $UAS\text{-}cac\text{-}eGFP^{786c}$ (22), $UAS\text{-}cac\text{-}eGFP^{422a}$ (22); SL: $UAS\text{-}cac\text{-}eGFP^{S/L(3\text{-}2M)}$, $UAS\text{-}cac\text{-}eGFP^{S/L(3\text{-}6M)}$, $UAS\text{-}cac\text{-}eGFP^{S/L(3\text{-}8M)}$; RQ: $UAS\text{-}cac\text{-}eGFP^{R/Q(1M)}$, $UAS\text{-}cac\text{-}eGFP^{R/Q(2\text{-}4M)}$; DM: $UAS\text{-}cac\text{-}eGFP^{DM(1M)}$, $UAS\text{-}cac\text{-}eGFP^{DM(2M)}$. After verifying similar expression levels for individual transgenic lines, those lines were used.

w^{1118} (92) was used as a non-transgenic wild-type control. The $itpr^{ug3}$ (93) and RyR^{E4340K} (63) mutant Drosophila stocks were obtained from the Bloomington Drosophila Stock Center (BDSC, Bloomington, Indiana). The *UAS-Plc21C(RNAi)* transformant lines 26557 and 26558 ($Plc21C^{GD11359}$) (94) were obtained from the Vienna Drosophila Resource Center (VDRC, Vienna, Austria). A $Gal80^{TS}$ expression line (35) was employed for a temporal Gal4 expression experiment. Flies were raised at 25°C (or 29°C for one temperature shift experiment) in humidity- and light-controlled Percival incubators (Geneva Scientific, Fontana, WI), in glass vials on a standard Drosophila food containing water, agar, molasses, yellow cornmeal, and yeast.

Electrophysiology and Analysis: Wandering third-instar larvae were selected for analysis. Larvae were dissected in a modified HL3 saline with the following components (and concentrations): NaCl (70 mM), KCl (5 mM), $MgCl_2$ (10 mM or 6 mM as noted), $NaHCO_3$ (10 mM), sucrose (115 mM = 3.9%), trehalose (4.2 mM = 0.16%), HEPES (5.0 mM = 0.12%), and $CaCl_2$ (0.5 mM, unless otherwise noted). Pharmacological agents tetrodotoxin (TTX, Tocris/R&D Systems), BAPTA-AM (Sigma), Xestospongin C (Tocris/R&D), or lithium chloride (LiCl, Sigma) were added as noted for some experiments. For the experiment using TTX (select agent toxin), all appropriate federal regulations and protocols established for the Select Agent Program established by the Centers for Disease Control and Prevention (CDC) and the US Department of Agriculture (USDA) were followed.

Electrophysiological data were collected using Axopatch 200B or Axoclamp 900A amplifiers (Molecular Devices, Sunnyvale, CA). Sharp electrode (> 10 MΩ) recordings were taken from muscle 6 of abdominal segments 2 and 3, as described previously (29, 30, 95). Prior to muscle V_m measurements, the Axoclamp 900A was bridge balanced. For the Axopatch 200B, the amplifier was placed in bridge mode (using I-CLAMP FAST for sharp electrode recordings). Before recording from each muscle, electrode resistance was measured and properly compensated by applying a step input and adjusting series resistance. Muscles with a V_m more hyperpolarized than -60 mV and an input resistance of greater than 5 MΩ were deemed suitable for recording (29). Data were digitized using a Digidata 1440A data acquisition system (Molecular Devices), and recorded using the pCLAMP 10 acquisition software (Molecular Devices). For presynaptic nerve stimulation, a Master-8 pulse stimulator (A.M.P. Instruments, Jerusalem, Israel) and an ISO-Flex isolation unit (A.M.P. Instruments) were utilized to deliver suprathreshold stimuli (1 ms unless otherwise indicated) to the appropriate segmental nerve. For each NMJ, the average amplitude of spontaneous miniature excitatory postsynaptic potential EPSPs (mEPSPs) was quantified by measuring approximately 100-200 individual spontaneous release events per NMJ. The average per-NMJ mEPSP amplitudes were then averaged for each genotype. Evoked EPSP amplitude was calculated for each NMJ as the average of 30 events (1 Hz). Quantal content (QC) was determined in two different ways. At low extracellular [Ca^{2+}], QC was calculated by the method of failures, as m = ln[(# trials)/(# failures)], as described elsewhere (38). At high extracellular [Ca^{2+}], QC was calculated by dividing EPSP/mEPSP, as described in the text. For analyses conducted across different calcium concentrations, QC was corrected for non-linear summation (96). For histograms displaying mEPSP amplitude frequencies, the same number of spontaneous events was analyzed for each NMJ (per genotype or experimental condition). This ensured that no individual NMJs were overrepresented or underrepresented in the aggregate analyses.

Immunostaining and Image Analysis: Third instar larvae were filleted in HL3 saline. Dissected animals were fixed for 3 minutes in Bouin's fixative (Ricca Chemical Company, Arlington, TX), washed using standard procedures, and incubated in primary antibodies overnight at 4°C. This was followed by

576 additional washes and a two-hour incubation in secondary antibody at room temperature. Staining was
577 performed using the following primary antibodies: mouse anti-GluRIIA (8B4D2) at 1:250 (bouton/cluster
578 counting) or 1:500 (intensity analyses) (Developmental Studies Hybridoma Bank (DSHB), University of
579 Iowa); rabbit anti-Dlg 1:30,000 (97, 98), mouse anti-Brp (nc82) 1:250 (32) (deposited to DSHB by
580 Buchner, E.), rabbit anti-GFP 1:250 (Torrey Pines Biolabs Inc. TP401). The following fluorophore-
581 conjugated antibodies were also used (Jackson ImmunoResearch Laboratories): goat anti-mouse-488
582 1:1000 (DyLight); and goat anti-rabbit-549 1:2000 (Dylight). Larval preparations were mounted in
583 Vectashield (Vector Laboratories) and imaged at room temperature using Zen software on a Zeiss 700
584 LSM mounted on an Axio Observer.Z1. An EC Plan-Neofluar 40X Oil DIC Objective (aperture 1.30) or an
585 EC Plan-Apochromat 63x Oil DIC Objective (aperture 1.40) (Carl Zeiss Microscopy) was used.

586 For analysis of fluorescence intensity and area, experimental and control larval preparations were
587 stained in the same container, mounted on the same slide, imaged using identical acquisition settings,
588 and analyzed using the same procedure and thresholds. Bouton and glutamate receptor cluster numbers
589 were quantified semi-automatically using the 'Spots' function in Imaris x64 v7.6.0 (Bitplane, Zurich
590 Switzerland). Any errors in automated counting were corrected by hand to arrive at the final value.
591 GluRIIA and Dlg levels were assessed using ImageJ 1.48s/Java 1.6.0_24 (64-bit) with Fiji plugins. Z-
592 stack images were compressed using the maximum projection function; ROIs were hand drawn to
593 exclude non-synaptic structures; a minimum threshold was set for each channel to eliminate background
594 fluorescence; and the Measure function was used to assess fluorescence intensity and area.

595 **Statistical Analyses and Data Plots:** Most electrophysiological comparisons were made across
596 multiple data sets. As appropriate, statistical significance was either assessed by one-way ANOVA with
597 Tukey's post-hoc analysis for multiple comparisons (Gaussian distribution), or a non-parametric Kruskal-
598 Wallis ANOVA with Dunn's post-hoc analysis for multiple comparisons (non-Gaussian distribution). Other
599 statistical tests utilized included Fisher's exact tests for viability counts or for statistical counts of gigantic
600 mEPSP events; Log-rank tests for survivability curves; linear regression analyses for calcium
601 cooperativity; and Student's T-Tests for direct comparisons between one control group and one

602 experimental group. *p* values of * $p < 0.05$, ** $p < 0.01$, *** $p < 0.001$, and **** $p < 0.0001$ were
603 considered significant. The values reported or plotted on regular bar graphs are mean ± SEM. The
604 values reported and plotted on box-and-whisker graphs are: box (25^{th} – 75^{th} percentiles), whiskers (1^{st} –
605 99^{th} percentiles), line (median), + symbol (average), and individual raw data points plotted outside the 1^{st}
606 and 99^{th} percentiles. Raw values for mEPSP electrophysiological data are given in Table 1. Statistical
607 analyses were performed in GraphPad Prism (GraphPad Software).
608
609
610
611 **ACKNOWLEDGEMENTS:** We thank Martin Müller, Chun-Fang Wu and members of the Frank lab for
612 helpful comments on earlier versions of this manuscript, and the laboratories of Tina Tootle and Fang Lin
613 for helpful discussions. We thank the Bloomington Drosophila Stock Center and the Vienna Drosophila
614 Resource Center for several fly stocks detailed in the Materials and Methods section.

615 **REFERENCES**
616
617 1. Kullmann DM. Neurological channelopathies. Annu Rev Neurosci. 2010;33:151-72.

618 2. Russell JF, Fu YH, Ptacek LJ. Episodic neurologic disorders: syndromes, genes, and
619 mechanisms. Annu Rev Neurosci. 2013;36:25-50.

620 3. Ryan DP, Ptacek LJ. Episodic neurological channelopathies. Neuron. 2010;68(2):282-92.

621 4. Ophoff RA, Terwindt GM, Vergouwe MN, van Eijk R, Oefner PJ, Hoffman SM, et al. Familial
622 hemiplegic migraine and episodic ataxia type-2 are caused by mutations in the Ca2+ channel gene
623 CACNL1A4. Cell. 1996;87(3):543-52.

624 5. Kors EE, Terwindt GM, Vermeulen FL, Fitzsimons RB, Jardine PE, Heywood P, et al. Delayed
625 cerebral edema and fatal coma after minor head trauma: role of the CACNA1A calcium channel subunit
626 gene and relationship with familial hemiplegic migraine. Ann Neurol. 2001;49(6):753-60.

627 6. Pietrobon D. Calcium channels and migraine. Biochimica et biophysica acta. 2013;1828(7):1655-
628 65.

629 7. Eikermann-Haerter K, Dilekoz E, Kudo C, Savitz SI, Waeber C, Baum MJ, et al. Genetic and
630 hormonal factors modulate spreading depression and transient hemiparesis in mouse models of familial
631 hemiplegic migraine type 1. The Journal of clinical investigation. 2009;119(1):99-109.

632 8. van den Maagdenberg AM, Pietrobon D, Pizzorusso T, Kaja S, Broos LA, Cesetti T, et al. A
633 Cacna1a knockin migraine mouse model with increased susceptibility to cortical spreading depression.
634 Neuron. 2004;41(5):701-10.

635 9. van den Maagdenberg AM, Pizzorusso T, Kaja S, Terpolilli N, Shapovalova M, Hoebeek FE, et al.
636 High cortical spreading depression susceptibility and migraine-associated symptoms in Ca(v)2.1 S218L
637 mice. Ann Neurol. 2010;67(1):85-98.

638 10. Kaja S, van de Ven RC, Broos LA, Veldman H, van Dijk JG, Verschuuren JJ, et al. Gene dosage-
639 dependent transmitter release changes at neuromuscular synapses of CACNA1A R192Q knockin mice
640 are non-progressive and do not lead to morphological changes or muscle weakness. Neuroscience.
641 2005;135(1):81-95.

642 11. Kaja S, Van de Ven RC, Broos LA, Frants RR, Ferrari MD, Van den Maagdenberg AM, et al.
643 Severe and progressive neurotransmitter release aberrations in familial hemiplegic migraine type 1
644 Cacna1a S218L knock-in mice. Journal of neurophysiology. 2010;104(3):1445-55.

645 12. Di Guilmi MN, Wang T, Inchauspe CG, Forsythe ID, Ferrari MD, van den Maagdenberg AM, et al.
646 Synaptic gain-of-function effects of mutant Cav2.1 channels in a mouse model of familial hemiplegic
647 migraine are due to increased basal [Ca2+]i. J Neurosci. 2014;34(21):7047-58.

648 13. Inchauspe CG, Urbano FJ, Di Guilmi MN, Ferrari MD, van den Maagdenberg AM, Forsythe ID, et
649 al. Presynaptic CaV2.1 calcium channels carrying familial hemiplegic migraine mutation R192Q allow
650 faster recovery from synaptic depression in mouse calyx of Held. Journal of neurophysiology.
651 2012;108(11):2967-76.

652 14. Inchauspe CG, Urbano FJ, Di Guilmi MN, Forsythe ID, Ferrari MD, van den Maagdenberg AM, et
653 al. Gain of function in FHM-1 Cav2.1 knock-in mice is related to the shape of the action potential. Journal
654 of neurophysiology. 2010;104(1):291-9.

15. Hullugundi SK, Ansuini A, Ferrari MD, van den Maagdenberg AM, Nistri A. A hyperexcitability phenotype in mouse trigeminal sensory neurons expressing the R192Q Cacna1a missense mutation of familial hemiplegic migraine type-1. Neuroscience. 2014;266:244-54.

16. Park J, Moon H, Akerman S, Holland PR, Lasalandra MP, Andreou AP, et al. Differential trigeminovascular nociceptive responses in the thalamus in the familial hemiplegic migraine 1 knock-in mouse: a Fos protein study. Neurobiology of disease. 2014;64:1-7.

17. Pietrobon D, Moskowitz MA. Pathophysiology of migraine. Annu Rev Physiol. 2013;75:365-91.

18. Vecchia D, Tottene A, van den Maagdenberg AM, Pietrobon D. Abnormal cortical synaptic transmission in CaV2.1 knockin mice with the S218L missense mutation which causes a severe familial hemiplegic migraine syndrome in humans. Frontiers in cellular neuroscience. 2015;9:8.

19. Vecchia D, Tottene A, van den Maagdenberg AM, Pietrobon D. Mechanism underlying unaltered cortical inhibitory synaptic transmission in contrast with enhanced excitatory transmission in CaV2.1 knockin migraine mice. Neurobiology of disease. 2014;69:225-34.

20. Inagaki A, Frank CA, Usachev YM, Benveniste M, Lee A. Pharmacological Correction of Gating Defects in the Voltage-Gated Cav2.1 Ca(2+) Channel due to a Familial Hemiplegic Migraine Mutation. Neuron. 2014;81(1):91-102.

21. Eikermann-Haerter K, Arbel-Ornath M, Yalcin N, Yu ES, Kuchibhotla KV, Yuzawa I, et al. Abnormal synaptic Ca(2+) homeostasis and morphology in cortical neurons of familial hemiplegic migraine type 1 mutant mice. Ann Neurol. 2015;78(2):193-210.

22. Kawasaki F, Zou B, Xu X, Ordway RW. Active zone localization of presynaptic calcium channels encoded by the cacophony locus of Drosophila. J Neurosci. 2004;24(1):282-5.

23. Lin DM, Goodman CS. Ectopic and increased expression of Fasciclin II alters motoneuron growth cone guidance. Neuron. 1994;13(3):507-23.

24. Brand AH, Perrimon N. Targeted gene expression as a means of altering cell fates and generating dominant phenotypes. Development. 1993;118(2):401-15.

25. Breen TR, Lucchesi JC. Analysis of the dosage compensation of a specific transcript in Drosophila melanogaster. Genetics. 1986;112(3):483-91.

26. Cline TW, Meyer BJ. Vive la difference: males vs females in flies vs worms. Annual review of genetics. 1996;30:637-702.

27. Lucchesi JC, Kuroda MI. Dosage compensation in Drosophila. Cold Spring Harbor perspectives in biology. 2015;7(5).

28. Fouquet W, Owald D, Wichmann C, Mertel S, Depner H, Dyba M, et al. Maturation of active zone assembly by Drosophila Bruchpilot. J Cell Biol. 2009;186(1):129-45.

29. Frank CA, Kennedy MJ, Goold CP, Marek KW, Davis GW. Mechanisms underlying the rapid induction and sustained expression of synaptic homeostasis. Neuron. 2006;52(4):663-77.

30. Frank CA, Pielage J, Davis GW. A presynaptic homeostatic signaling system composed of the Eph receptor, ephexin, Cdc42, and CaV2.1 calcium channels. Neuron. 2009;61(4):556-69.

31. Gaviño MA, Ford KJ, Archila S, Davis GW. Homeostatic synaptic depression is achieved through a regulated decrease in presynaptic calcium channel abundance. eLife. 2015;4.

32. Wagh DA, Rasse TM, Asan E, Hofbauer A, Schwenkert I, Durrbeck H, et al. Bruchpilot, a protein with homology to ELKS/CAST, is required for structural integrity and function of synaptic active zones in Drosophila. Neuron. 2006;49(6):833-44.

33. DiAntonio A, Petersen SA, Heckmann M, Goodman CS. Glutamate receptor expression regulates quantal size and quantal content at the Drosophila neuromuscular junction. J Neurosci. 1999;19(8):3023-32.

34. Feng Y, Ueda A, Wu CF. A modified minimal hemolymph-like solution, HL3.1, for physiological recordings at the neuromuscular junctions of normal and mutant Drosophila larvae. Journal of neurogenetics. 2004;18(2):377-402.

35. McGuire SE, Le PT, Osborn AJ, Matsumoto K, Davis RL. Spatiotemporal rescue of memory dysfunction in Drosophila. Science. 2003;302(5651):1765-8.

36. Jan LY, Jan YN. Properties of the larval neuromuscular junction in Drosophila melanogaster. J Physiol. 1976;262(1):189-214.

37. Martin AR. Quantal Nature of Synaptic Transmission. Physiol Rev. 1966;46:51-66.

38. Del Castillo J, Katz B. Quantal components of the end-plate potential. J Physiol. 1954;124(3):560-73.

39. Frank CA. Homeostatic plasticity at the Drosophila neuromuscular junction. Neuropharmacology. 2014;78:63-74.

40. Frank CA. How voltage-gated calcium channels gate forms of homeostatic synaptic plasticity. Frontiers in cellular neuroscience. 2014;8:40.

41. Brusich DJ, Spring AM, Frank CA. A single-cross, RNA interference-based genetic tool for examining the long-term maintenance of homeostatic plasticity. Frontiers in cellular neuroscience. 2015;9:107.

42. Shortridge RD, Yoon J, Lending CR, Bloomquist BT, Perdew MH, Pak WL. A Drosophila phospholipase C gene that is expressed in the central nervous system. J Biol Chem. 1991;266(19):12474-80.

43. Tedford HW, Zamponi GW. Direct G protein modulation of Cav2 calcium channels. Pharmacol Rev. 2006;58(4):837-62.

44. Cremona O, De Camilli P. Phosphoinositides in membrane traffic at the synapse. Journal of cell science. 2001;114(Pt 6):1041-52.

45. Goni FM, Alonso A. Structure and functional properties of diacylglycerols in membranes. Progress in lipid research. 1999;38(1):1-48.

46. Huang FD, Woodruff E, Mohrmann R, Broadie K. Rolling blackout is required for synaptic vesicle exocytosis. J Neurosci. 2006;26(9):2369-79.

47. Peters C, Bayer MJ, Buhler S, Andersen JS, Mann M, Mayer A. Trans-complex formation by proteolipid channels in the terminal phase of membrane fusion. Nature. 2001;409(6820):581-8.

730 48. Rohrbough J, Broadie K. Lipid regulation of the synaptic vesicle cycle. Nat Rev Neurosci.
731 2005;6(2):139-50.

732 49. Wu L, Bauer CS, Zhen XG, Xie C, Yang J. Dual regulation of voltage-gated calcium channels by
733 PtdIns(4,5)P2. Nature. 2002;419(6910):947-52.

734 50. Dahdal D, Reeves DC, Ruben M, Akabas MH, Blau J. Drosophila pacemaker neurons require g
735 protein signaling and GABAergic inputs to generate twenty-four hour behavioral rhythms. Neuron.
736 2010;68(5):964-77.

737 51. Llano I, Gonzalez J, Caputo C, Lai FA, Blayney LM, Tan YP, et al. Presynaptic calcium stores
738 underlie large-amplitude miniature IPSCs and spontaneous calcium transients. Nat Neurosci.
739 2000;3(12):1256-65.

740 52. Liu Q, Chen B, Yankova M, Morest DK, Maryon E, Hand AR, et al. Presynaptic ryanodine
741 receptors are required for normal quantal size at the Caenorhabditis elegans neuromuscular junction. J
742 Neurosci. 2005;25(29):6745-54.

743 53. Collin T, Marty A, Llano I. Presynaptic calcium stores and synaptic transmission. Curr Opin
744 Neurobiol. 2005;15(3):275-81.

745 54. Emptage NJ, Reid CA, Fine A. Calcium stores in hippocampal synaptic boutons mediate short-
746 term plasticity, store-operated Ca2+ entry, and spontaneous transmitter release. Neuron.
747 2001;29(1):197-208.

748 55. Simkus CR, Stricker C. The contribution of intracellular calcium stores to mEPSCs recorded in
749 layer II neurones of rat barrel cortex. J Physiol. 2002;545(Pt 2):521-35.

750 56. Wong CO, Chen K, Lin YQ, Chao Y, Duraine L, Lu Z, et al. A TRPV channel in Drosophila motor
751 neurons regulates presynaptic resting Ca2+ levels, synapse growth, and synaptic transmission. Neuron.
752 2014;84(4):764-77.

753 57. Joshi R, Venkatesh K, Srinivas R, Nair S, Hasan G. Genetic dissection of itpr gene function
754 reveals a vital requirement in aminergic cells of Drosophila larvae. Genetics. 2004;166(1):225-36.

755 58. Conti R, Tan YP, Llano I. Action potential-evoked and ryanodine-sensitive spontaneous Ca2+
756 transients at the presynaptic terminal of a developing CNS inhibitory synapse. J Neurosci.
757 2004;24(31):6946-57.

758 59. Dunn TW, Syed NI. Ryanodine receptor-transmitter release site coupling increases quantal size
759 in a synapse-specific manner. The European journal of neuroscience. 2006;24(6):1591-605.

760 60. Gordon GR, Bains JS. Noradrenaline triggers multivesicular release at glutamatergic synapses in
761 the hypothalamus. J Neurosci. 2005;25(49):11385-95.

762 61. Sharma G, Vijayaraghavan S. Modulation of presynaptic store calcium induces release of
763 glutamate and postsynaptic firing. Neuron. 2003;38(6):929-39.

764 62. Dunn TW, McCamphill PK, Syed NI. Activity-induced large amplitude postsynaptic mPSPs at
765 soma-soma synapses between Lymnaea neurons. Synapse. 2009;63(2):117-25.

766 63. Dockendorff TC, Robertson SE, Faulkner DL, Jongens TA. Genetic characterization of the 44D-
767 45B region of the Drosophila melanogaster genome based on an F2 lethal screen. Molecular & general
768 genetics : MGG. 2000;263(1):137-43.

64. Hallcher LM, Sherman WR. The effects of lithium ion and other agents on the activity of myo-inositol-1-phosphatase from bovine brain. J Biol Chem. 1980;255(22):10896-901.

65. Lenox RH, Wang L. Molecular basis of lithium action: integration of lithium-responsive signaling and gene expression networks. Mol Psychiatry. 2003;8(2):135-44.

66. Gafni J, Munsch JA, Lam TH, Catlin MC, Costa LG, Molinski TF, et al. Xestospongins: potent membrane permeable blockers of the inositol 1,4,5-trisphosphate receptor. Neuron. 1997;19(3):723-33.

67. Wilcox RA, Primrose WU, Nahorski SR, Challiss RA. New developments in the molecular pharmacology of the myo-inositol 1,4,5-trisphosphate receptor. Trends Pharmacol Sci. 1998;19(11):467-75.

68. Goswami SP, Bucurenciu I, Jonas P. Miniature IPSCs in hippocampal granule cells are triggered by voltage-gated Ca2+ channels via microdomain coupling. J Neurosci. 2012;32(41):14294-304.

69. Ermolyuk YS, Alder FG, Surges R, Pavlov IY, Timofeeva Y, Kullmann DM, et al. Differential triggering of spontaneous glutamate release by P/Q-, N- and R-type Ca2+ channels. Nat Neurosci. 2013;16(12):1754-63.

70. Xu-Friedman MA, Regehr WG. Maximinis. Nat Neurosci. 2000;3(12):1229-30.

71. Melom JE, Akbergenova Y, Gavornik JP, Littleton JT. Spontaneous and evoked release are independently regulated at individual active zones. J Neurosci. 2013;33(44):17253-63.

72. Yao WD, Wu CF. Auxiliary Hyperkinetic beta subunit of K+ channels: regulation of firing properties and K+ currents in Drosophila neurons. J Neurophysiol. 1999;81(5):2472-84.

73. Berke BA, Lee J, Peng IF, Wu CF. Sub-cellular Ca2+ dynamics affected by voltage- and Ca2+-gated K+ channels: Regulation of the soma-growth cone disparity and the quiescent state in Drosophila neurons. Neuroscience. 2006;142(3):629-44.

74. Gao Z, Todorov B, Barrett CF, van Dorp S, Ferrari MD, van den Maagdenberg AM, et al. Cerebellar ataxia by enhanced Ca(V)2.1 currents is alleviated by Ca2+-dependent K+-channel activators in Cacna1a(S218L) mutant mice. J Neurosci. 2012;32(44):15533-46.

75. Vanmolkot KR, Kors EE, Turk U, Turkdogan D, Keyser A, Broos LA, et al. Two de novo mutations in the Na,K-ATPase gene ATP1A2 associated with pure familial hemiplegic migraine. European journal of human genetics : EJHG. 2006;14(5):555-60.

76. Bergquist S, Dickman DK, Davis GW. A hierarchy of cell intrinsic and target-derived homeostatic signaling. Neuron. 2010;66(2):220-34.

77. Lee J, Ueda A, Wu CF. Pre- and post-synaptic mechanisms of synaptic strength homeostasis revealed by slowpoke and shaker K+ channel mutations in Drosophila. Neuroscience. 2008;154(4):1283-96.

78. Lee J, Ueda A, Wu CF. Distinct roles of Drosophila cacophony and Dmca1D Ca(2+) channels in synaptic homeostasis: genetic interactions with slowpoke Ca(2+) -activated BK channels in presynaptic excitability and postsynaptic response. Developmental neurobiology. 2014;74(1):1-15.

79. Peng IF, Wu CF. Drosophila cacophony channels: a major mediator of neuronal Ca2+ currents and a trigger for K+ channel homeostatic regulation. J Neurosci. 2007;27(5):1072-81.

807 80. Parrish JZ, Kim CC, Tang L, Bergquist S, Wang T, Derisi JL, et al. Kruppel mediates the selective
808 rebalancing of ion channel expression. Neuron. 2014;82(3):537-44.

809 81. Li P, Chen SR. Molecular basis of Ca(2)+ activation of the mouse cardiac Ca(2)+ release channel
810 (ryanodine receptor). The Journal of general physiology. 2001;118(1):33-44.

811 82. Rahman T. Dynamic clustering of IP3 receptors by IP3. Biochemical Society transactions.
812 2012;40(2):325-30.

813 83. Zahradnik I, Gyorke S, Zahradnikova A. Calcium activation of ryanodine receptor channels--
814 reconciling RyR gating models with tetrameric channel structure. The Journal of general physiology.
815 2005;126(5):515-27.

816 84. Laver DR. Ca2+ stores regulate ryanodine receptor Ca2+ release channels via luminal and
817 cytosolic Ca2+ sites. Clinical and experimental pharmacology & physiology. 2007;34(9):889-96.

818 85. de Vries B, Eising E, Broos LA, Koelewijn SC, Todorov B, Frants RR, et al. RNA expression
819 profiling in brains of familial hemiplegic migraine type 1 knock-in mice. Cephalalgia : an international
820 journal of headache. 2014;34(3):174-82.

821 86. Drissi H, Lasmoles F, Le Mellay V, Marie PJ, Lieberherr M. Activation of phospholipase C-beta1
822 via Galphaq/11 during calcium mobilization by calcitonin gene-related peptide. J Biol Chem.
823 1998;273(32):20168-74.

824 87. Morara S, Wang LP, Filippov V, Dickerson IM, Grohovaz F, Provini L, et al. Calcitonin gene-
825 related peptide (CGRP) triggers Ca2+ responses in cultured astrocytes and in Bergmann glial cells from
826 cerebellar slices. Eur J Neurosci. 2008;28(11):2213-20.

827 88. Drissi H, Lieberherr M, Hott M, Marie PJ, Lasmoles F. Calcitonin gene-related peptide (CGRP)
828 increases intracellular free Ca2+ concentrations but not cyclic AMP formation in CGRP receptor-positive
829 osteosarcoma cells (OHS-4). Cytokine. 1999;11(3):200-7.

830 89. Goadsby PJ, Edvinsson L, Ekman R. Release of vasoactive peptides in the extracerebral
831 circulation of humans and the cat during activation of the trigeminovascular system. Ann Neurol.
832 1988;23(2):193-6.

833 90. Goadsby PJ, Edvinsson L, Ekman R. Vasoactive peptide release in the extracerebral circulation
834 of humans during migraine headache. Ann Neurol. 1990;28(2):183-7.

835 91. Kaiser EA, Russo AF. CGRP and migraine: could PACAP play a role too? Neuropeptides.
836 2013;47(6):451-61.

837 92. Hazelrigg T, Levis R, Rubin GM. Transformation of white locus DNA in drosophila: dosage
838 compensation, zeste interaction, and position effects. Cell. 1984;36(2):469-81.

839 93. Deshpande M, Venkatesh K, Rodrigues V, Hasan G. The inositol 1,4,5-trisphosphate receptor is
840 required for maintenance of olfactory adaptation in Drosophila antennae. J Neurobiol. 2000;43(3):282-8.

841 94. Dietzl G, Chen D, Schnorrer F, Su KC, Barinova Y, Fellner M, et al. A genome-wide transgenic
842 RNAi library for conditional gene inactivation in Drosophila. Nature. 2007;448(7150):151-6.

843 95. Davis GW, DiAntonio A, Petersen SA, Goodman CS. Postsynaptic PKA controls quantal size and
844 reveals a retrograde signal that regulates presynaptic transmitter release in Drosophila. Neuron.
845 1998;20(2):305-15.

96. Martin AR. A further study of the statistical composition on the end-plate potential. J Physiol. 1955;130(1):114-22.

97. Budnik V, Koh YH, Guan B, Hartmann B, Hough C, Woods D, et al. Regulation of synapse structure and function by the Drosophila tumor suppressor gene dlg. Neuron. 1996;17(4):627-40.

98. Pielage J, Cheng L, Fetter RD, Carlton PM, Sedat JW, Davis GW. A presynaptic giant ankyrin stabilizes the NMJ through regulation of presynaptic microtubules and transsynaptic cell adhesion. Neuron. 2008;58(2):195-209.

854 **FIGURE LEGENDS**

855

856 **Figure 1: SL- and DM-expressing flies exhibit coarse phenotypes. (A)** Schematic of Ca_V2-type
857 calcium channel α1a subunit, with substitutions to Drosophila Cacophony (Cac) residues indicated
858 (mammalian numbering in parentheses) and a CLUSTAL-Omega alignment of Cac, human CACNA1A,
859 and mouse CACNA1A amino acids spanning the relevant region ([*] - fully conserved residue; [:] -
860 strongly similar; [.] - weakly similar). **(B-C)** Visible phenotypes for larvae resulting from crosses of
861 *elaV(C155)-Gal4* females x *Balancer Chrom/UAS-cac*$^{MUT\ or\ WT}$ males. **(B)** Premature spiracle protrusion in
862 larvae expressing the *UAS-cac*^{SL} (shown) or *UAS-cac*^{DM} (not shown) transgenic lines. The spiracle
863 phenotype does not occur in larvae expressing *UAS-cac*^{RQ} or *UAS-cac*^{WT}. **(C)** Same crosses as in (B)
864 showing diminished *UAS-cac* mutant viability. "*UAS-cac* Viability Index" = # *UAS-cac* transgenic adult
865 progeny/# Balancer Chromosome siblings, normalized to 100% for WT female progeny counts (see
866 Table 1 for raw progeny counts; for all *UAS-cac* comparisons, $n \geq 115$ Balancer sibling progeny were
867 counted). Male and female progeny were considered separately due to possible sex differences. *** $p <$
868 0.001 by Fisher's Exact test compared to WT sex-specific control. # $p = 0.05$, ### $p < 0.001$ by Fisher's
869 Exact test between sexes for the SL or DM genotypes. **(D, E)** For both males and females, there was
870 starkly diminished longevity for adult flies expressing the DM transgene. **** $p < 0.0001$ by Log-rank test.

871

872 **Figure 2: Neuronal expression and synaptic localization of Cac-GFP are normal. (A-D)** Images of
873 larval central nervous systems for animals expressing Cac-GFP WT or mutant transgenes. Anti-GFP
874 (red), and anti-Bruchpilot (Brp - green) staining are shown. Scale bar 100 μm. **(E)** Per unit area in
875 neurons, there is no significant difference in neuronal Cac-GFP intensity across the transgenic lines (*ns* –
876 not significant, $p = 0.50$ by one-way ANOVA, and $p > 0.6$ for all possible Tukey's post-hoc comparisons).
877 **(F-I)** Transgenic Cac-GFP proteins successfully localize to NMJ active zones, as indicated by co-staining
878 with anti-Brp (green) and anti-GFP (red). Scale bar 5 μm. **(J)** For DM-expressing NMJs, synaptic bouton
879 numbers are normal, except for slight undergrowth for synapse A2 muscle 6/7 (* $p < 0.05$, Student's T-

880 test vs. WT, $n \geq 8$ NMJs for all genotypes and segments). **(K)** The number of glutamate receptor clusters
881 per synapse at DM-expressing NMJs is not statistically different than WT-expressing NMJs ($p > 0.1$,
882 Student's T-test, $n \geq 8$ NMJs for all genotypes and segments). **(L-M)** For DM-expressing NMJs, there is a
883 small increase in GluRIIA-containing receptor area coverage (L) and for anti-GluRIIA staining intensity
884 normalized for anti-Dlg intensity (M) (* $p < 0.05$ by Student's T-test vs. WT for both measures, $n \geq 15$
885 NMJs for each genotype).

886

887 **Figure 3: SL- and DM-expressing flies display hyperexcitability in evoked neurotransmission. (A)**
888 Average EPSP amplitudes at 0.4 mM $[Ca^{2+}]_e$. for non-transgenic control (w^{1118}) or various Cac-GFP-
889 expressing lines (** $p < 0.01$ by one-way ANOVA with Tukey's post-hoc vs. w^{1118}; # $p < 0.05$ and ### $p <$
890 0.001 vs. WT; $n \geq 12$ for all genotypes,). **(B)** Average quantal content (QC estimated as EPSP/mEPSP)
891 at 0.4 mM $[Ca^{2+}]_e$ ($p > 0.15$ by one-way ANOVA with Tukey's post-hoc for all genotypes, compared to
892 both w^{1118} and WT controls). **(C)** Log-log plots of extracellular calcium concentration vs. QC corrected for
893 non-linear summation (NLS QC). There are no statistically significant differences in calcium cooperativity
894 between genotypes ($p = 0.16$ by linear regression analysis). **(D, E)** Example electrophysiological traces
895 of **(D)** normal and **(E)** abnormal EPSP waveforms. **(F)** Effect of genotype on EPSP waveforms in
896 response to 30 presynaptic pulses: normal, extra discharge, and shoulders categories. "RQ only"
897 signifies larvae with a null endogenous *cac* mutation rescued to viability by the RQ-expressing
898 transgene. **(G)** Effect of genotype on number of extra discharges observed per 30 presynaptic pulses (* p
899 < 0.05 and *** $p < 0.001$ vs. WT by one-way Kruskal-Wallis ANOVA with Dunn's post-hoc). **(H)**
900 Penetrance and **(I)** severity of DM-associated extra discharge waveform dysfunction in low extracellular
901 Mg^{2+} (6 mM). All genotypes abbreviated (WT, DM, SL, RQ) are *elaV(C155)-Gal4/Y; UAS-cac-eGFP*$^{(X)}$/+
902 or w^{1118} for non-transgenic wild type. Data bars represent the average value and error bars the SEM.

903

Figure 4: SL- and DM-expressing NMJs have enhanced mEPSPs. (A) Electrophysiological traces of spontaneous activity at WT- and DM-expressing NMJs. Example traces with two different scales are shown to display the variable severity of spontaneous neurotransmission phenotypes. **(B)** Effects of genotype on average mEPSP amplitude. ** $p < 0.01$ vs. w^{1118} by one-way ANOVA with Tukey's post-hoc; # $p < 0.05$, ### $p < 0.001$ vs. WT by one-way ANOVA with Tukey's post-hoc. **(C)** Effects of genotype on mEPSP frequency. ### $p < 0.001$ vs. WT by one-way ANOVA with Tukey's post-hoc; $n \geq 12$ NMJs, all genotypes. **(D)** Box and whisker plots of mEPSP amplitude range at 0.5 mM extracellular Ca^{2+}. Box denotes 25^{th}-75^{th} percentile; line denotes median; + sign denotes average; whiskers range from 1^{st}-99^{th} percentile; individual data points outside the 1^{st} and 99^{th} percentiles are also plotted; (*** $p < 0.001$ by Kruskal-Wallis ANOVA with Dunn's post-hoc vs. either w^{1118} or WT; $n > 1400$ mEPSPs for each genotype). **(E)** Cumulative probability histogram of the same data as (D) showing a marked rightward shift in mEPSP amplitudes for SL- and DM-expressing NMJs. **(F)** Box and whisker plot (data as in (D)) of mEPSP amplitude range when expressing the DM transgene for acute periods of developmental time (*** $p < 0.001$ by Kruskal-Wallis ANOVA with Dunn's post-hoc vs. DM 0 hr, ### $p < 0.001$ by vs. DM 24 hr; $n > 1095$ mEPSPs for each genotype). **(G)** Cumulative probability histogram of the same data in (F) showing a rightward shift in mEPSP amplitudes for longer periods of DM expression.

Figure 5: Gigantic spontaneous events vanish in response to diminished Ca^{2+}, buffered Ca^{2+}, or blocked Na_V function. (A) Box and whisker plot of mEPSP amplitudes at 0.2 mM extracellular Ca^{2+}. Plot as in Fig. 4 (*** $p < 0.001$ by Kruskal-Wallis ANOVA with Dunn's post-hoc vs. either w^{1118} or WT; $n > 780$ mEPSPs for each genotype). **(B)** Cumulative probability histogram of the same data as (A) showing a rightward shift in mEPSP amplitudes for SL- and DM-expressing NMJs – but less so than for 0.5 mM Ca^{2+} in Figure 4. **(C-E)** Cumulative probability histograms of mEPSP size separately showing the effects of zero extracellular Ca^{2+} (C); application of BAPTA-AM in 0.5 mM Ca^{2+} (D); application of TTX in 0.5 mM Ca^{2+} (E). For each case, the rightward shift in mEPSP size distribution persists due to DM expression. However, the gigantic spontaneous events are eliminated (arrowheads). **(F)** Box and whisker plots

930 demonstrating elimination of gigantic spontaneous events. *** $p < 0.001$ by Fisher's exact test examining
931 the incidence of gigantic mEPSPs > 10 mV vs. DM or SL alone, as appropriate).

932

933 **Figure 6: Failure analysis - SL- and DM-expressing NMJs show elevated release probability at**
934 **very low extracellular calcium. (A-B)** Frequencies of evoked amplitudes at very low extracellular Ca^{2+}
935 (0.14 mM) for **(A)** WT-expressing NMJs and **(B)** DM-expressing NMJs. For the DM-expressing NMJs,
936 there is a clear rightward shift in the size distribution of DM-expressing events, as well as a marked
937 decrease in the frequency of failures (categorized as 0 mV events). **(C)** Further lowering extracellular
938 Ca^{2+} (0.1 mM) for DM reveals a leftward shift in size distribution and an increase in failure percentage
939 compared to (B). **(D)** For WT-, DM-, and SL-expressing NMJs, the average EPSP size for successfully
940 evoked events, as well as estimated QC for by failure analyses (0.14 mM Ca^{2+}). * $p < 0.05$; ** $p < 0.01$ by
941 one-way ANOVA with Tukey's post-hoc compared to WT. **(E)** Box and whisker plots for both failure
942 analysis and spontaneous events. Data are presented as in Figures 4 and 5 – this time showing the size
943 distributions of spontaneous mEPSP events (WT, DM, SL), as well as failure analysis (FA) evoked
944 events for the same genotypes (failures excluded).

945

946 **Figure 7: Inhibition of an intracellular Ca^{2+} release pathway dampens gain-of-function phenotypes**
947 **associated with FHM1-mimicking mutations. (A)** Schematic of an RNA interference (RNAi)-based
948 approach to identify suppressors of gain-of-function electrophysiological phenotypes. **(B)** Knockdown of
949 *Plc21C* gene function reverses the increase in spontaneous mEPSP amplitude elicited by DM
950 expression. **(C)** Box and whisker plots (as before) and **(D-E)** cumulative probability histograms (as
951 before) demonstrate that heterozygous, loss-of-function point mutations in genes encoding the IP_3
952 receptor ($Itpr^{\mu g3}$) and the Ryanodine receptor (RyR^{E4340K}) also diminish the gain-of-function spontaneous
953 mEPSP phenotypes in DM-expressing NMJs. *** $p < 0.001$ by Kruskal-Wallis ANOVA with Dunn's
954 multiple comparisons test vs. DM alone. **(F)** The RyR^{E4340K} mutation also diminishes evoked EPSP

hyperexcitability phenotypes in a DM-expressing background (# of extra discharges [ED] per muscle – see also Figure 3).

Figure 8: Pharmacological inhibition of intracellular Ca2+ release dampens gain-of-function phenotypes associated with FHM1-mimicking mutations. (A-C) Data displayed and analyzed as before. Box and whisker plots (A) and cumulative probability histograms (B-C) demonstrate that acute application of either LiCl (to block PIP_2 recycling) or Xestospongin C (to block IP_3 receptors) both suppress the gain-of-function spontaneous mEPSP phenotypes in DM-expressing NMJs. *** $p < 0.001$ by Kruskal-Wallis ANOVA with Dunn's multiple comparisons test vs. DM alone. **(D)** Cartoon model depicting neuronal components implicated in this study of regulating neurophysiology downstream of migraine-mimicking amino-acid substitutions. Red – Ca_V2 channels; gray – IP_3 receptors; blue – Ryanodine receptors; yellow – Na_V channels.

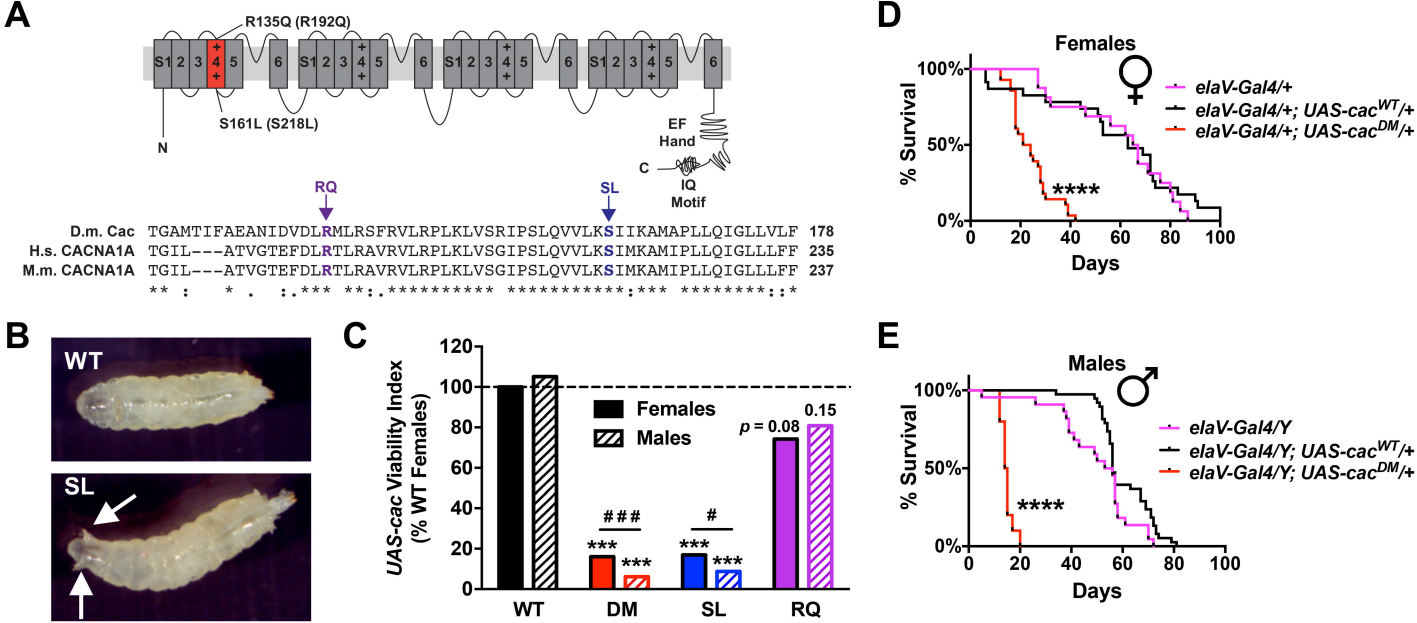
A
R135Q (R192Q)
S161L (S218L)
N
C
EF Hand
IQ Motif
RQ
SL
D.m. Cac TGAMTIFAEANIDVDLRMLRSFRVLRPLKLVSRIPSLQVVLKSIIKAMAPLLQIGLLVLF 178
H.s. CACNA1A TGIL---ATVGTEFDLRTLRAVRVLRPLKLVSGIPSLQVVLKSIMKAMIPLLQIGLLLFF 235
M.m. CACNA1A TGIL---ATVGTEFDLRTLRAVRVLRPLKLVSGIPSLQVVLKSIMKAMIPLLQIGLLLFF 237
B
WT
SL
C
UAS-cac Viability Index (% WT Females)
Females
Males
p = 0.08
0.15
###
#
***
WT
DM
SL
RQ
D
Females
% Survival
Days
elaV-Gal4/+
elaV-Gal4/+; UAS-cacWT/+
elaV-Gal4/+; UAS-cacDM/+
****
E
Males
elaV-Gal4/Y
elaV-Gal4/Y; UAS-cacWT/+
elaV-Gal4/Y; UAS-cacDM/+

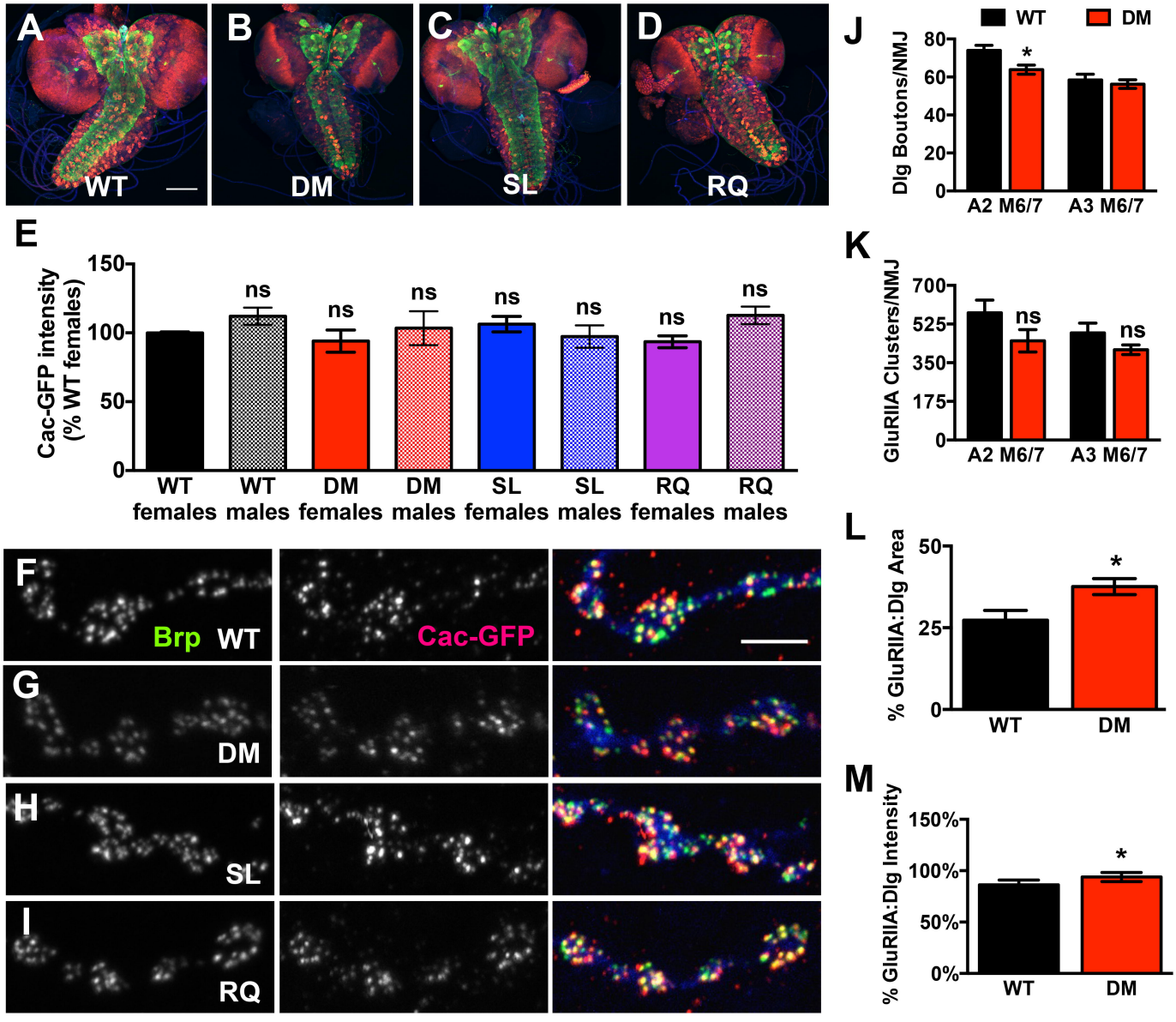
A
WT
B
DM
C
SL
D
RQ
J
WT
DM
Dlg Boutons/NMJ
80
60
40
20
0
*
A2 M6/7
A3 M6/7
E
Cac-GFP intensity (% WT females)
150
100
50
0
ns
WT females
WT males
DM females
DM males
SL females
SL males
RQ females
RQ males
K
GluRIIA Clusters/NMJ
700
525
350
175
0
ns
A2 M6/7
A3 M6/7
F
Brp WT
Cac-GFP
G
DM
H
SL
I
RQ
L
% GluRIIA:Dlg Area
50
25
0
*
WT
DM
M
% GluRIIA:Dlg Intensity
150%
100%
50%
0%
*
WT
DM

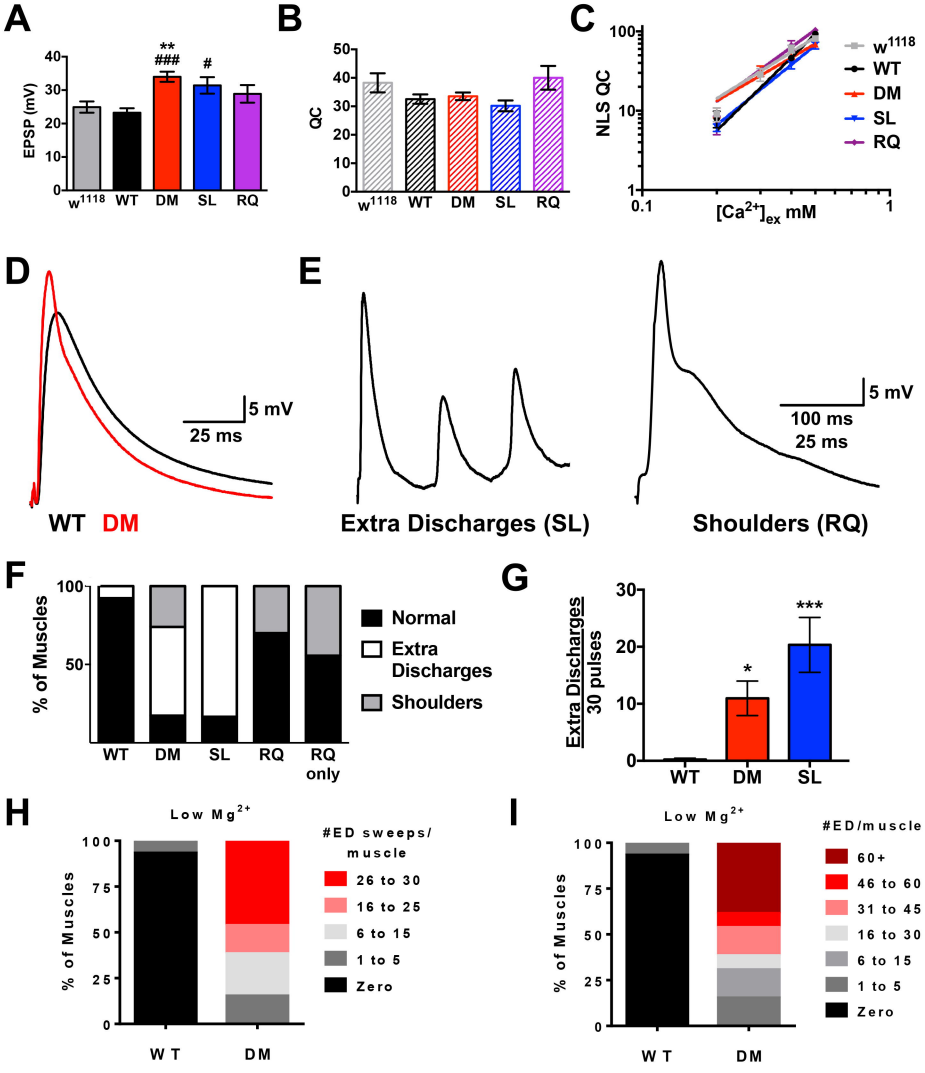
A
EPSP (mV)
40
30
20
10
0
**
###
#
w1118 WT DM SL RQ
B
QC
50
40
30
20
10
0
w1118 WT DM SL RQ
C
NLS QC
100
10
1
0.1
[Ca2+]ex mM
1
w1118
WT
DM
SL
RQ
D
5 mV
25 ms
WT DM
E
5 mV
100 ms
25 ms
Extra Discharges (SL)
Shoulders (RQ)
F
% of Muscles
100
50
WT DM SL RQ RQ only
Normal
Extra Discharges
Shoulders
G
Extra Discharges / 30 pulses
30
20
10
0
*
***
WT DM SL
H
Low Mg2+
% of Muscles
100
75
50
25
0
W T DM
#ED sweeps/ muscle
26 to 30
16 to 25
6 to 15
1 to 5
Zero
I
Low Mg2+
% of Muscles
100
75
50
25
0
W T DM
#ED/muscle
60+
46 to 60
31 to 45
16 to 30
6 to 15
1 to 5
Zero

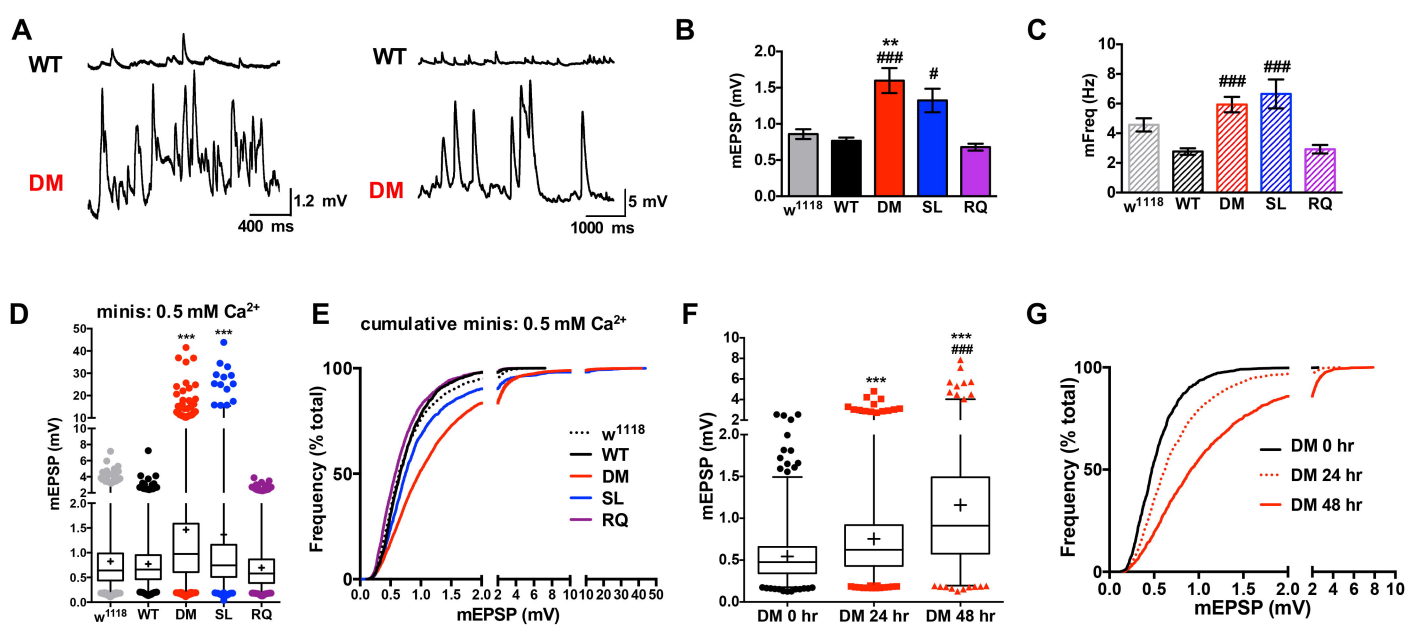
A
WT
DM
1.2 mV
400 ms
WT
DM
5 mV
1000 ms
B
mEPSP (mV)
**
###
#
w1118
WT
DM
SL
RQ
C
mFreq (Hz)
###
###
w1118
WT
DM
SL
RQ
D
minis: 0.5 mM Ca2+
mEPSP (mV)
***
***
w1118
WT
DM
SL
RQ
E
cumulative minis: 0.5 mM Ca2+
Frequency (% total)
w1118
WT
DM
SL
RQ
mEPSP (mV)
F
mEPSP (mV)
***
***
###
DM 0 hr
DM 24 hr
DM 48 hr
G
Frequency (% total)
DM 0 hr
DM 24 hr
DM 48 hr
mEPSP (mV)

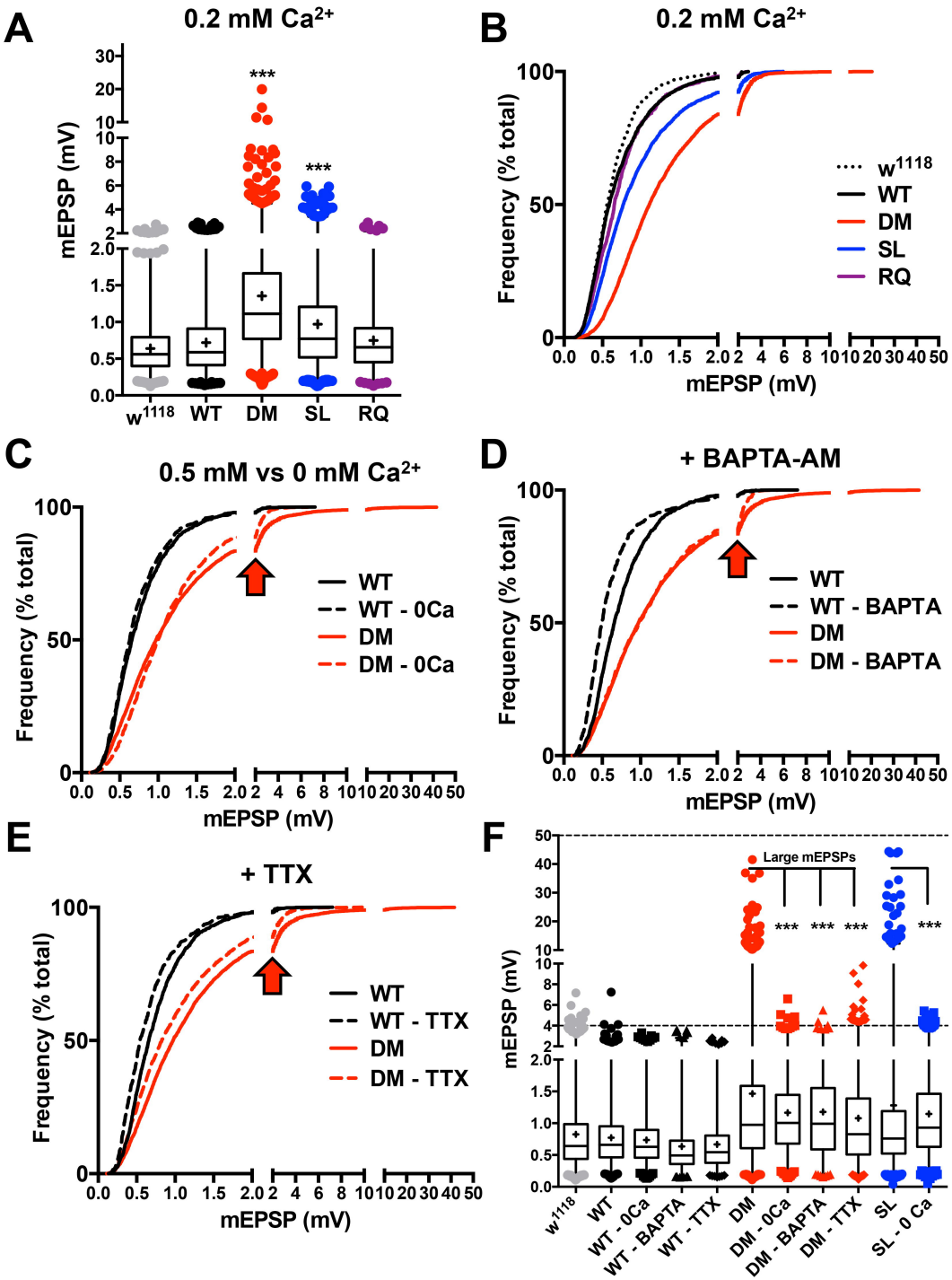
A
0.2 mM Ca2+
mEPSP (mV)
***
***
w1118
WT
DM
SL
RQ
B
0.2 mM Ca2+
Frequency (% total)
w1118
WT
DM
SL
RQ
mEPSP (mV)
C
0.5 mM vs 0 mM Ca2+
Frequency (% total)
WT
WT - 0Ca
DM
DM - 0Ca
mEPSP (mV)
D
+ BAPTA-AM
Frequency (% total)
WT
WT - BAPTA
DM
DM - BAPTA
mEPSP (mV)
E
+ TTX
Frequency (% total)
WT
WT - TTX
DM
DM - TTX
mEPSP (mV)
F
Large mEPSPs
***
mEPSP (mV)
w1118
WT
WT - 0Ca
WT - BAPTA
WT - TTX
DM
DM - 0Ca
DM - BAPTA
DM - TTX
SL
SL - 0 Ca

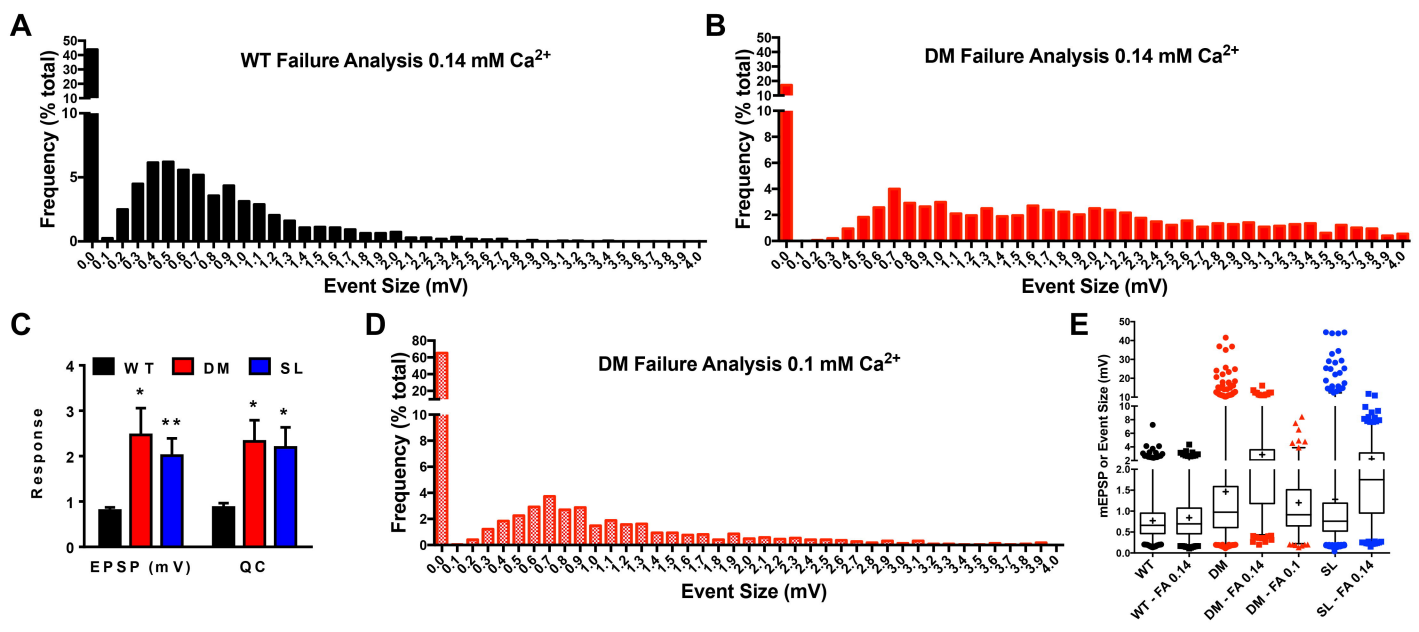
A
WT Failure Analysis 0.14 mM Ca2+
Frequency (% total)
Event Size (mV)
B
DM Failure Analysis 0.14 mM Ca2+
Frequency (% total)
Event Size (mV)
C
WT
DM
SL
Response
EPSP (mV)
QC
D
DM Failure Analysis 0.1 mM Ca2+
Frequency (% total)
Event Size (mV)
E
mEPSP or Event Size (mV)
WT
WT - FA 0.14
DM
DM - FA 0.14
DM - FA 0.1
SL
SL - FA 0.14

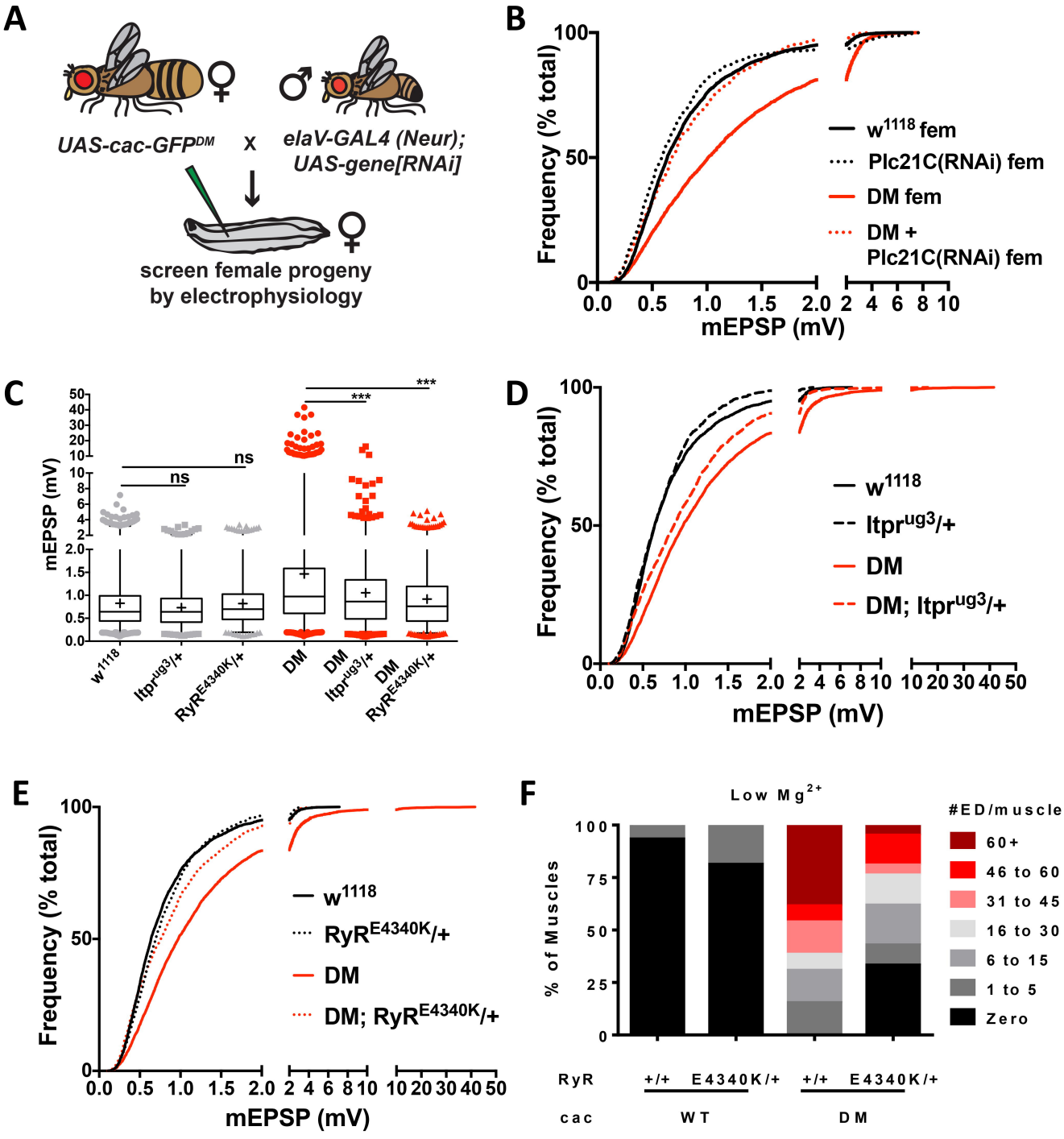
A
UAS-cac-GFP^DM
x
elaV-GAL4 (Neur);
UAS-gene[RNAi]
screen female progeny
by electrophysiology
B
Frequency (% total)
mEPSP (mV)
w1118 fem
Plc21C(RNAi) fem
DM fem
DM +
Plc21C(RNAi) fem
C
mEPSP (mV)
ns
ns
***
***
w1118
Itpr ug3/+
RyR E4340K/+
DM
DM
Itpr ug3/+
DM
RyR E4340K/+
D
Frequency (% total)
mEPSP (mV)
w1118
Itpr ug3/+
DM
DM; Itpr ug3/+
E
Frequency (% total)
mEPSP (mV)
w1118
RyR E4340K/+
DM
DM; RyR E4340K/+
F
Low Mg2+
% of Muscles
#ED/muscle
60+
46 to 60
31 to 45
16 to 30
6 to 15
1 to 5
Zero
RyR
+/+
E4340K/+
+/+
E4340K/+
cac
WT
DM

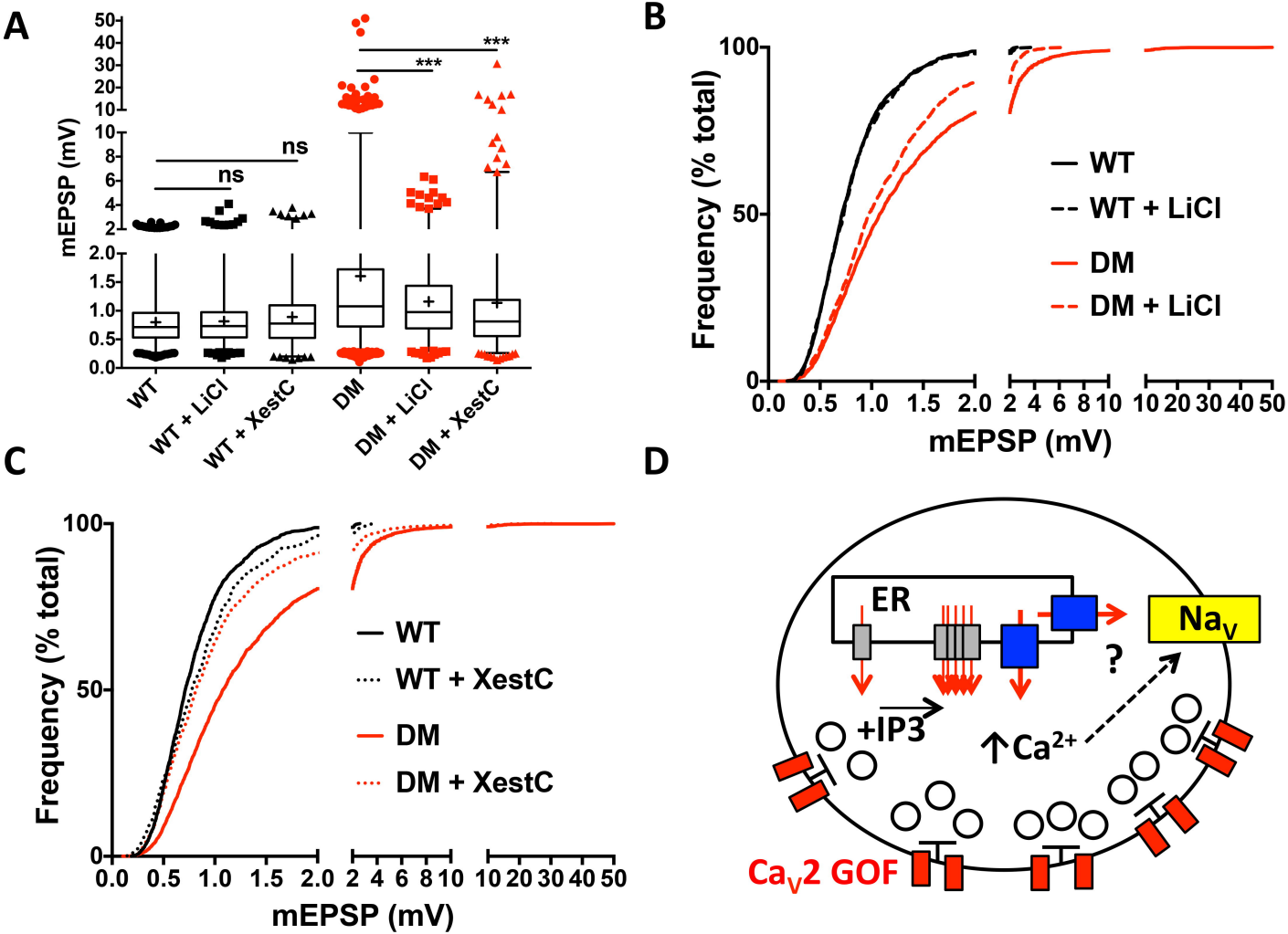
A
mEPSP (mV)
ns
ns
***
***
WT
WT + LiCl
WT + XestC
DM
DM + LiCl
DM + XestC
B
Frequency (% total)
mEPSP (mV)
WT
WT + LiCl
DM
DM + LiCl
C
Frequency (% total)
mEPSP (mV)
WT
WT + XestC
DM
DM + XestC
D
ER
Na$_V$
?
+IP3
↑Ca^{2+}
Ca$_V$2 GOF